Remote Sensing of Environment 266 (2021) 112676

Contents lists available at ScienceDirect

Remote Sensing of Environment

journal homepage: www.elsevier.com/locate/rse

Early detection of spruce vitality loss with hyperspectral data: Results of an experimental study in Bavaria, Germany

Kathrin Einzmann [a,b], Clement Atzberger [a], Nicole Pinnel [c], Christina Glas [a], Sebastian Böck [a], Rudolf Seitz [b], Markus Immitzer [a,*]

[a] University of Natural Resources and Life Sciences, Vienna (BOKU), Institute of Geomatics, Peter-Jordan-Straße 82, 1190 Vienna, Austria
[b] Bavarian State Institute of Forestry (LWF), Department of Information Technology, Research Group: Remote Sensing, Hans-Carl-von-Carlowitz-Platz 1, 85354 Freising, Germany
[c] German Aerospace Center (DLR), German Remote Sensing Data Center (DFD), International Ground Segment, Münchner Straße 20, 82234 Weßling, Germany

ARTICLE INFO

Edited by: Marie Weiss

Keywords:
Hyperspectral data
Forest health
Vitality loss
Random Forest
Ring-barking

ABSTRACT

Vitality loss of trees caused by extreme weather conditions, drought stress or insect infestations, are expected to increase with ongoing climate change. The detection of vitality loss at an early stage is thus of vital importance for forestry and forest management to minimize ecological and economical damage. Remote sensing instruments are able to detect changes over large areas down to the level of individual trees. The scope of our study is to investigate whether it is possible to detect stress-related spectral changes at an early stage using hyperspectral sensors. For this purpose, two Norway spruce (*Picea abies*) forest stands, both different in age and maintenance, were monitored in the field over two vegetation periods. In parallel, time series of airborne hyperspectral remote sensing data were acquired. For each stand 70 trees were artificially stressed (ring-barked) and 70 trees were used as control trees. The data collected in south-eastern Germany consists of measurements at multiple times and at different scales: (1) crown conditions were visually assessed in the field (2) needle reflectance spectra were acquired in the laboratory using a FieldSpec spectrometer, and (3) hyperspectral airborne data (HySpex) were flown at 0.5 m spatial resolution. We aimed for a simultaneous data acquisition at the three levels. This unique data set was investigated whether any feature can be discriminated to detect vitality loss in trees at an early stage. Several spectral transformations were applied to the needle and tree crown spectra, such as spectral derivatives, vegetation indices and angle indices. All features were examined for their separability (ring-barked vs. control trees) with the Random Forest (RF) classification algorithm. As result, the younger, well maintained forest stand only showed minor changes over the 2-year period, whereas changes in the older forest stand were observable both in the needle and in the hyperspectral tree crown spectra, respectively. These changes could even be detected before changes were visible by field observations. The tree spectral reactions to ring-barking were first noticeable 11 months after ring-barking and 6 weeks before they were visible by field inspection. The most discriminative features for separating the two groups were the reflectance spectra and the spectral derivatives, over the VIs or angle indices. The tree crown spectra of the two groups could be separated by the RF classifier with a 79% overall accuracy at the beginning of the second vegetation period and 1 month later with 92% overall accuracy with high kappa index. The results clearly demonstrate the great potential of hyperspectral remote sensing in detecting early vitality changes of stressed trees.

1. Introduction

Natural disturbances, such as fires, insect outbreaks and windthrows, play an important role in forest ecosystems with major ecological as well as economic impacts. Due to changing climate conditions the disturbance activity is expected to further increase in the near future (Seidl et al., 2020, 2017).

To better understand ecosystem functions, but also to ensure sustainable forest management, forest disturbances are one of the main research topics in forestry and ecology. Earth observation (EO) can make a significant and cost-efficient contribution in this area as it can provide spatially accurate and yet large-scale information on the extent of the

* Corresponding author.
E-mail address: markus.immitzer@boku.ac.at (M. Immitzer).

https://doi.org/10.1016/j.rse.2021.112676
Received 3 May 2021; Received in revised form 26 July 2021; Accepted 23 August 2021
Available online 21 September 2021

disturbances quickly after the event. The remotely derived information also provides essential input for ecological models as well as for management recommendations. In recent years, the well-known potential of EO has led to an increased use of various remote sensing platforms and sensors for the detection of forest disturbances, also summarized in several review studies (Atzberger et al., 2020; Lausch et al., 2017, 2016; Rullan-Silva et al., 2013; Senf et al., 2017).

Typically, disturbances that significantly change the forest canopy can be well identified. Examples are the detection of burned areas (Barbosa et al., 1999; Giglio et al., 2009; Gitas et al., 2008; Pereira, 2003; Roy et al., 2005; Weirather et al., 2018), windthrows (Chehata et al., 2014; Einzmann et al., 2017; Elatawneh et al., 2014) but also the mapping of older bark beetle outbreaks where the trees already show strong discolorations, e.g. red or grey-attack (Coggins et al., 2011; Fernandez-Carrillo et al., 2020; Franklin et al., 2003; Havašová et al., 2015; Immitzer and Atzberger, 2014; Wulder et al., 2009; Zimmermann and Hoffmann, 2020). In the case of infestation by biotic pests, however, the early detection of infested trees is paramount. Only intervention at this stage helps to prevent further spread and large outbreaks (Wermelinger, 2004). This is also the case for bark beetle infestation on spruce, which is currently one of the most problematic disturbances in Central Europe.

To tackle this problem, increased efforts have been devoted over the past 10 years to detect the so-called green-attack phases of bark beetle infestation which only manifests in small and subtle spectral changes (Abdullah et al., 2019, 2018; Fassnacht et al., 2014, 2012; Immitzer and Atzberger, 2014; Lausch et al., 2013). The spectral data for the analysis of the aforementioned small spectral changes were collected either through needle sampling (e.g. Abdullah et al., 2018; Cheng et al., 2010; Einzmann et al., 2014; Reichmuth et al., 2018), by UAVs (e.g., Immitzer et al., 2017; Klouček et al., 2019; Näsi et al., 2018, 2015; Safonova et al., 2019), aircrafts (e.g., Fassnacht et al., 2014; Lausch et al., 2013; Niemann et al., 2015) or satellites (e.g., Abdullah et al., 2019; Immitzer and Atzberger, 2014; Meddens et al., 2013). Several of these studies show the potential of high-quality state-of-the-art remote sensing sensors with high to very high spectral resolution. The same studies also highlight the often-limited spatial resolution of the employed sensors which do not allow an analysis of individual tree crowns. It is well known, however, that next to the spectral resolution a finer spatial resolution can lead to higher mapping accuracies (Lausch et al., 2013; Näsi et al., 2018).

The task is further exuberated by the fact that natural ecosystems often react very differently to biotic disturbances. The infestation of bark beetles, for example, depends on the one hand on the development of the beetle population, which is strongly driven by the weather, and on the other hand on the resistance of the trees. Furthermore, it is possible that the typical sequence of green, red and grey-attack does not occur and that the trees lose their needles even before the discoloration (i.e. no red-attack is observed). It also has to be considered, that spectro-temporal signatures of forests are highly variable due to different growing conditions, highly variable stand characteristics (e.g. age structure, canopy density, crown coverage,) and different management regimes (Grabska and Socha, 2021; Schlerf and Atzberger, 2006). Even without taking disturbances into account, the research community still struggles to correctly model the optical properties of forest canopies (Widlowski et al., 2015). Together, this makes early detection of infestation using EO more difficult and explains why no operational bark beetle detection systems are yet available (Atzberger et al., 2020; Zimmermann and Hoffmann, 2020).

The scope of this study is the early detection of stress-induced spectral changes in Norway spruce stand with hyperspectral data. Compared to other studies, the experimental set-up was optimized to better cover and characterize the stress period. To simulate a bark beetle infestation, trees were manually stressed by removal of the bark, phloem and cambium (ring-barking). This treatment interrupts the phloem sap flow from the needles to the roots. A ring-barked spruce tree will die after 1–3 years (Roth et al., 2001). The ring-barking simulates a bark beetle infestation as the Spruce beetles infest the phloem-cambial region of tree and the larvae starts to feed on the phloem. By feasting on the vital tree's bast fibre, the infested trees start to die off (Foster et al., 2017; Seybold et al., 2008). Nearby trees from a control group were left unchanged and two forests were chosen to assess the impact of tree age. Data were repeatedly collected over two vegetation periods at three different scales: (i) field observations to visually assess crown conditions, (ii) needle sampling and laboratory needle reflectance spectra (ASD FieldSpec), and (iii) hyperspectral airborne (HySpex) data with sub-meter spatial resolution. A part of this experiment and preliminary results were published in Reichmuth et al. (2018) who analyzed needle spectra of eight ring-barked trees and eight control trees for assessing the separability of the two groups using spectral reflectance, vegetation indices and derivative analysis.

Using this unique data set, we investigate the following research questions

1) Is it possible to reliably detect vitality changes in spruce forests with hyperspectral data on needle and crown level?
2) When are changes in the spectral behavior due to ring-barking first noticeable?
3) Which are the most discriminative spectral features?
4) Are findings related to tree age?

2. Material and methods

The study involved a large amount of terrestrial, laboratory and airborne data (Fig. 1). The data are described in the next sub-sections, along with a description of the study site and the methods employed for data analysis.

2.1. Test site

A test site near the town of Altötting (48°13′N, 12°43′E) in Bavaria, Germany was selected for this study (Fig. 2). For our analysis, two spruce forest stands of different age were selected:

- $\text{Stand}_{\text{young}}$ ("Gaderbogen"): a 60 year old forest stand, well-maintained with an even thinning
- $\text{Stand}_{\text{old}}$ ("Einsiedl"): an 80–100 year old forest stand, denser with unevenly spaced trees

Both forest stands are located on flat terrain approximately 415 m above sea level. The forests grow on calcareous gravel fields from the last glacial period covered with weak podzolic luvisol providing good root penetration and nutrition. The potential natural vegetation is a beech forest with few oaks. The current vegetation is spruce in monoculture stands. The ground cover mainly consists of wood small-reed (*Calamagrostis epigejos*), European blackberry (*Rubus fruticosus* agg.) and European red raspberry (*Rubus idaeus*) (LWF, 2014).

The climate of the study area is subcontinental with a mean temperature of 7.8 °C and a yearly mean precipitation of 940 mm (1998–2013). The mean vegetation period (days above 10 °C daily average temperature) is 158 days per year (LWF, 2014). Detailed climate analysis shows in particular that the first year of experiments started with a colder winter, but temperatures began to rise from April onwards to above the long-term average. During the vegetation period (April till October), the average air temperature for both years was higher (13.8 °C in 2013; 14.0 °C in 2014) compared to the long-term average (12.6 °C).

2.2. Experimental stress induction in Spruce trees by ring-barking

To ensure sufficiently stressed trees next to healthy trees, we artificially stressed trees using the ring-barking (girdling) method (Noel, 1970). Ring-barking was conducted manually with a bark stripper (debarker) removing an approximate 20 cm broad bark stripe at breast

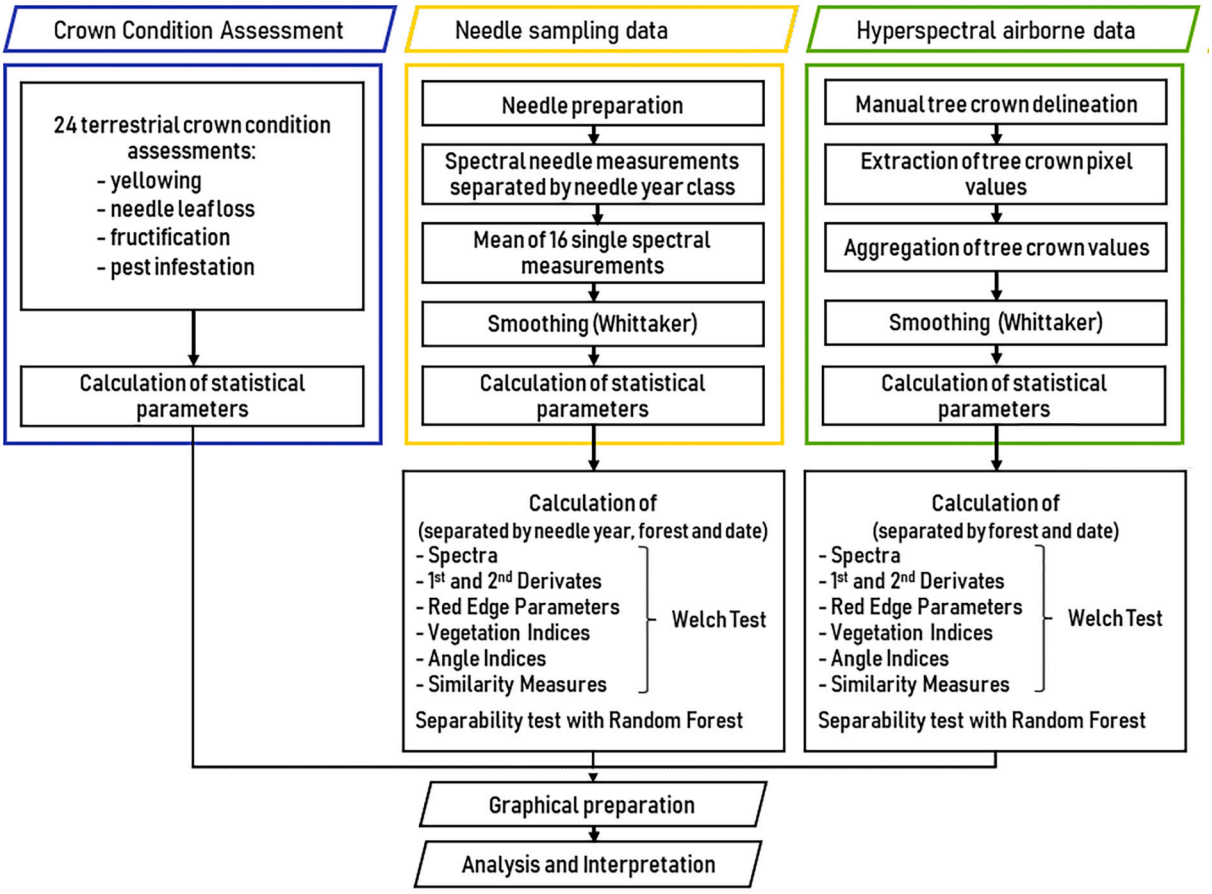

Fig. 1. Overview of main data sources and processing steps.

height (Fig. 2). This damage disrupts the nutrient flow from the needles to the roots and negatively influences the vitality of the tree. Healthy (control) trees were selected in near-by locations to ensure similar growing conditions (see Fig. 2). While selecting the trees for the study (both the deliberately stressed and the healthy trees), care was taken to select predominantly pre-mating trees with a sufficiently large crown, to ensure unbiased findings and to facilitate the spectral measurements.

In each of the two forest stands, 140 trees have been monitored. All trees were uniquely numbered and their position was measured using a GPS device. On each site, 70 trees were ring-barked and 70 control trees remained untreated. The trees were ring-barked on 13 June 2013 and monitored until August 2014.

2.3. Data acquisition and preprocessing

The data acquisition started in May 2013 and included multiple levels: Satellite data, aircraft data, sampling in tree crowns, and ground-based crown condition assessment. Great care was taken to synchronise the field activities with the remote sensing data acquisitions. The data acquisition was mainly done in the summer months. The crown condition assessments were performed as often as possible by a forester. For the needle sampling a field campaign with tree climbers and several people on the ground were needed. The hyperspectral data acquisitions were scheduled once a week but were highly dependent on weather conditions. WorldView-2 data were taken three times in 2013 and three times in 2014. However, due to unfavourable weather conditions and suboptimal acquisition parameters (mainly too large off-nadir angles), this data was not included in the analysis. It has also to be noted that bark beetle infestation occurred in early summer 2014 which led to the felling of the affected trees and to the end of the experiment in July 2014.

An overview of the data acquisition can be found in the result chapter (Fig. 5).

2.3.1. Crown condition assessment

Terrestrial crown conditions were assessed 24 times, visually appraising the tree vitality. The quality of the crown condition assessment depends heavily on the visibility of the tree crown. This information is important in order to be able to make conclusions about the reliability of the crown assessment. The visibility of the tree was noted and classified in one of the five classes reaching from “entire crown clearly visible” to “crown not visible”. Recorded vitality measures included yellowing, needle leaf loss, fructification and pest infestation. Yellowing was recorded in 5% increments. Needle leaf loss was estimated and recorded as well in 5% increments and assigned to five damage classes reaching from “without damage” to “dead”. Fructification was addressed in four stages reaching from “no fructification” to “strong fructification”. A distinction was made between old and new fructification, as well as the stage of development of the new fructification. Pest infestation for each tree was noted as well, specifying the type of damage and if possible, the vermin. The foresters used field glasses for the crown condition assessment and monitored each tree each time from the same position. More criteria which are not relevant for this study (for example strength classes) were noted. A detailed description of the crown condition assessment is given in the standard recommendations by Bavarian State Institute of Forestry (LWF, 2012).

2.3.2. Needle spectra measurement

In each forest stand, eight trees were selected for sampling: four control trees and four ring-barked trees. The sampling was done seven

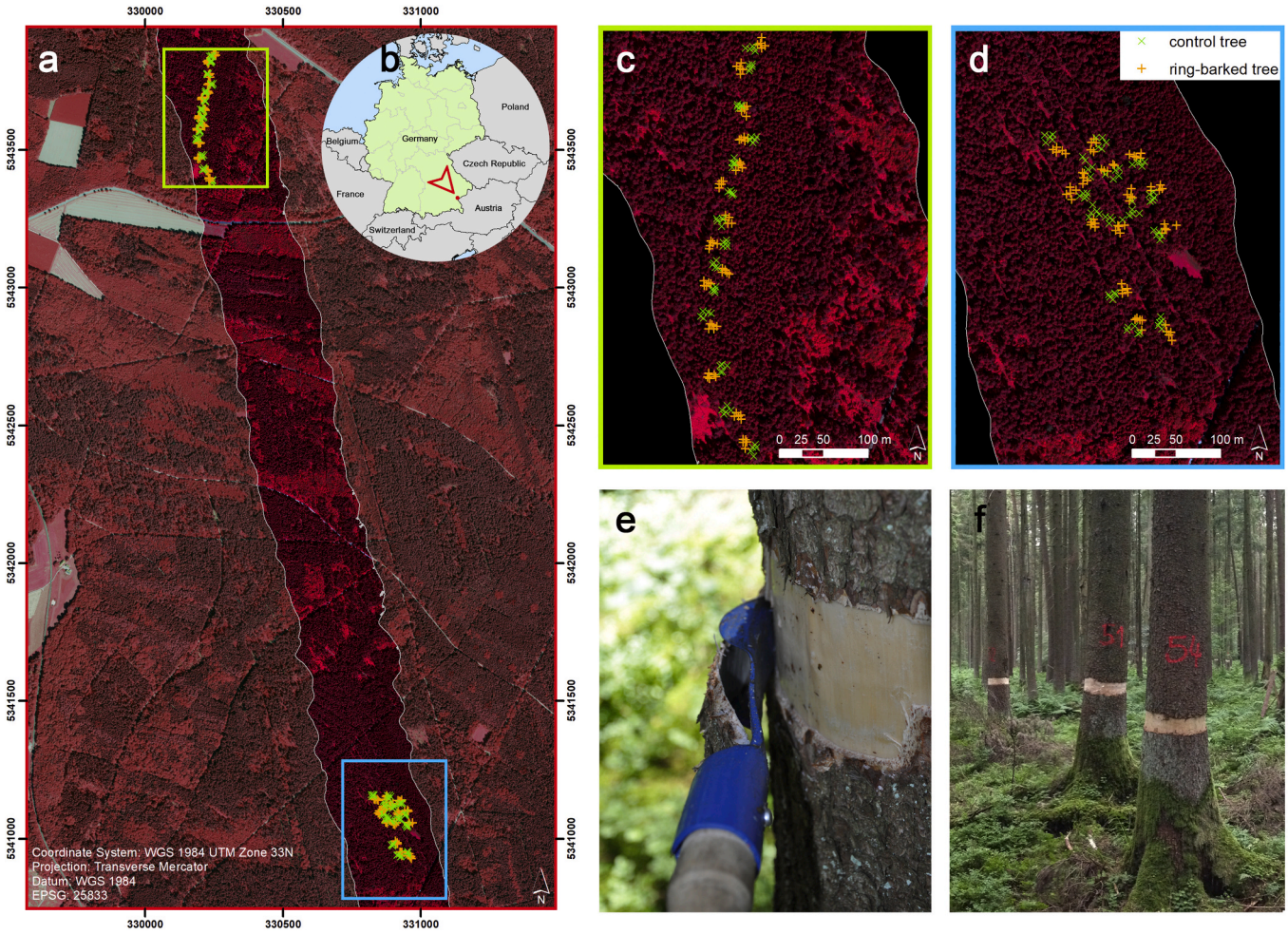

Fig. 2. CIR composition of the test site using HySpex flight line from 5 Aug 2013 (RGB = bands 124, 68,33; grey border) and orthoimage in the background (a). Location of the test site in South-Germany (b) and detail views of the young (c) and old stand (d) with the control and ring-barked trees. Ring-barking process (e) and group of ring-barked trees (f).

times during the study period (four times in 2013, three times in 2014). Experienced tree climbers cut down 1–2 branches per probed tree from the sun-lit crown. On site, the branches were subdivided into twigs of the last four vegetation periods (2010–2013, see Fig. 3). The twigs per vegetation period were immediately refrigerated and brought to the lab. On the following day, the needles were cut from the twigs and measured separately for each tree and each vegetation period with an ASD FieldSpec Pro FR spectrometer (Analytical Spectral Devices, Inc., Boulder, CO, US), covering the range 350–2500 nm. For the spectral measurements of the needle samples, a contact probe was used, which measures directly on the needle surface (see Fig. 3). Using a contact probe over a dense stack of needles ensures obtaining pure needle spectra. Each needle spectrum consists of a mean of 16 single spectral measurements.

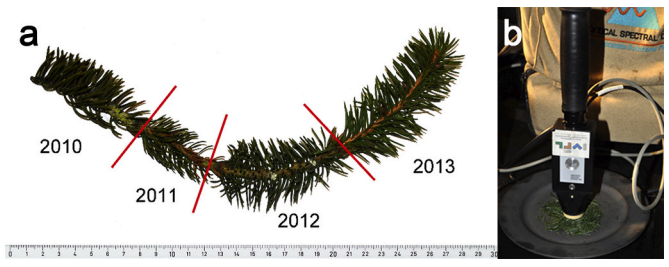

Fig. 3. Needle sampling and measurement: Needle age classes 2010–2013 (a) and spectral measurement with the contact probe (b).

The ASD spectrometer was selected to ensure that all channels of the aircraft-mounted hyperspectral sensors are covered (see Table 1). For details of needle collection and needle measurements see Einzmann et al. (2014). This work highlighted also the importance of a separated analyses of the needle age classes.

2.3.3. *Hyperspectral airborne data acquisition*

The hyperspectral data were collected from an imaging spectrometer system being mounted on a Cessna C 208 aircraft. The aircraft had a flight height of approximately 600 m and was operated by the German Aerospace Center (DLR) in Oberpfaffenhofen. The imaging spectrometer system consists of two individual HySpex sensors from Norsk Elektro Optic. The visible and near infrared (VNIR) spectral domain is recorded by HySpex VNIR-1600 and the short-wave infrared (SWIR) domain is covered by SWIR-320 m-e (Köhler, 2016). Details are reported in Table 1. Since there is an overlap of the two sensors (968–992 nm), the

Table 1
Main HySpex sensor characteristics (based on Köhler (2016)).

HySpex sensor	VNIR-1600	SWIR-320 m-e
Spectral range	416–992 nm	994 (968[a])–2498 nm
Spectral bands	160	252 (256[a])
Spectral sampling interval	3.6 nm	6 nm
Field of view (FOV)	16.7°	13.2°
Spatial resolution at 600 m above ground	0.5 m	1 m

[a] The first four channels have been removed.

first four channels of the SWIR sensor have been removed, resulting in a total of 412 analyzed channels. During the experimental period, the study area was overflown eleven times (green dots in Fig. 5).

The hyperspectral sensor surveys were conducted eight times in 2013 (once before ring-barking) and three times in 2014. The data was preprocessed at DLR using well-established processing routines (Habermeyer et al., 2005; Holzwarth et al., 2011; Krauß et al., 2013), leading to top-of-canopy spectral bi-directional reflectances. The processing steps included an automatic system correction, a parametrical orthorectification (Müller et al., 2005), merging of the data of both sensors and a scene-based atmospheric correction (ATCOR) (Richter et al., 2011). Data taken within the ozone and water vapor absorption regions (760 nm, 940 nm, 1130 nm, 1400 nm and 1900 nm) were removed and refilled with interpolated values. As part of the georectification, the data of the SWIR sensor with 1 m spatial resolution were resampled to 0.5 m resulting in the same spatial resolution as VNIR data and merged to a full data cube. Finally, quality control was carried out (Bachmann et al., 2007).

Based on the GPS measurements the corresponding tree crown were selected and to minimize shadow influences, the well-lit part of the tree crown of all monitored trees were manually delineated in all hyperspectral airborne data sets (Fig. 4). Afterwards, mean reflectance spectra of the individual tree crowns were extracted.

2.4. Hyperspectral data smoothing and feature extraction

To minimize noise, the extracted data were smoothed with a modified Whittaker Smoother (Atzberger and Eilers, 2011). We used standard settings of the Whittaker smoother with lambda set to 10 and using the 2nd derivative for roughness calculations. After application of the Whittaker smoother, first and second order derivatives were calculated from the needle and HySpex spectra using first difference transformation (FDR) (Dawson and Curran, 1998). The analysis of the derivatives helps to distinguish spectral features that would otherwise not be visible in the original spectral signatures. Derivatives are also usually more robust against illumination differences compared to the input spectra (Tsai and Philpot, 1998).

To further enhance different traits of the vegetation cover (e.g., leaf area index (LAI), water content, cell structure, leaf chlorophyll content), fifteen vegetation indices (VIs) were calculated (Table 2), for both needle and HySpex data. The calculated VIs can be separated in four groups:

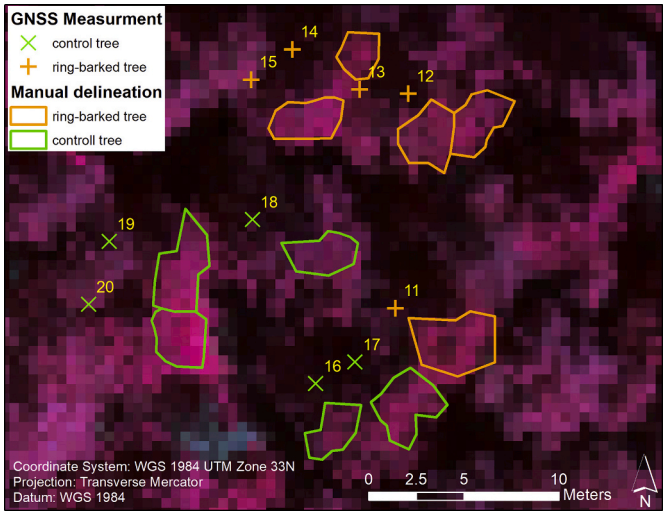

Fig. 4. Example for the manual delineation of tree crowns (polygons) in $Stand_{old}$ for the airborne HySpex data from 05 August 2013 (CIR composition: RGB = bands 124, 68,33).

Table 2
Vegetation indices used for the present study.

Index	Equation	Reference
Leaf pigment and canopy density indices		
Greenness Index	$GI = \frac{R(554)}{R(677)}$	Smith et al. (1995)
Modified Chlorophyll Absorption Ratio Index	$MCARI = [(R700) - R(670)) - 0.2*(R(700) - R(550)] * \frac{R(700)}{R(670)}$	Daughtry et al. (2000)
Modified Red Edge Simple Ratio	$MRESR = \frac{R(750) - R(445)}{R(750) - R(445)}$	Datt (1999), Sims and Gamon (2002)
Normalized Difference Lignin Index	$NDLI = \frac{log\left(\frac{1}{R(1754)}\right) - log\left(\frac{1}{R(1680)}\right)}{log\left(\frac{1}{R(1754)}\right) + log\left(\frac{1}{R(1680)}\right)}$	Fourty et al. (1996), Melillo et al. (1982), Serrano et al. (2002)
Normalized Difference Vegetation Index	$NDVI = \frac{R(800) - R(680)}{R(800) + R(680)}$	Rouse et al. (1974)
Photochemical Reflectance Index	$PRI = \frac{R(531) - R(570)}{R(531) + R(570)}$	Gamon et al. (1997, 1992)
Plant Senescence Reflectance Index	$PSRI = \frac{R(677) - R(500)}{R(750)}$	Merzlyak et al. (1999)
Red Edge Normalized Difference Vegetation Index	$RENDVI = \frac{R(750) - R(705)}{R(750) + R(705)}$	Gitelson and Merzlyak (1994)
Water stress indices		
Normalized Difference Infrared Index	$NDII = \frac{R(819) - R(1649)}{R(819) + R(1649)}$	Hardisky et al. (1983)
Normalized Difference Water Index	$NDWI = \frac{R(857) - R(1241)}{R(857) + R(1241)}$	Gao (1996)
Water Band Index	$WBI = \frac{R(970)}{R(900)}$	Champagne et al. (2001), Penuelas et al. (1993)
Angle indices (*)		
Angle at NIR	$ANIR\ (\alpha_{NIR}) = cos^{-1}\left(\frac{a^2 + b^2 + c^2}{2*a*b}\right)$	Khanna et al. (2007)
Shortwave Angle Slope Index	$SASI\ (\beta_{SWIR1}) = cos^{-1}\left(\frac{a^2 + b^2 + c^2}{2*a*b}\right)*$ $slope$ $slope = SWIR2 - NIR$	Palacios-Orueta et al. (2006)
Red edge indices		
Red Edge Inflection Point $REIP_{FDR}$ (**)	$R' = \frac{dR}{dW} = \frac{reflectance\ band_{i+1} - reflectance\ band_i}{wavelenght\ band_{i+1} - wavelenght\ band_i}$ $R'' = \frac{d2R}{dW2} = \frac{d}{dW}\left(\frac{dR}{dW}\right)$	Dawson and Curran (1998), Mutanga and Skidmore (2007)
Red Edge Inflection Point $REIP_{Guyot}$	$REIP_{Guyot} = 700 + 40* \left[\frac{\frac{R(670) + R(780)}{2} - R(700)}{R(740) - R(700)}\right]$	Guyot et al. (1988)

The thirteen indices were broadly subdivided in 'leaf pigment and canopy density indices', 'water stress indies', 'angle indices' and 'red edge indices'.
(*) For ANIR a, b and c are Euclidian distances between the vertices RED (R646) and NIR(R858), NIR and SWIR1(R1237), and RED and SWIR1 (Palacios-Orueta et al., 2006). Whereas for SASI a, b and c are Euclidian distances between the vertices NIR(R858) and SWIR1(R1237), SWIR1 and SWIR2(R1639), and NIR and SWIR2 (Khanna et al., 2007).
(**) $REIP_{FDR}$ = R' is the 1st derivative and R'' is the 2nd derivative. dR is the difference of reflectance of spectral $band_{i+1}$ and spectral $band_i$. dW corresponds to the difference in wavelength between spectral $band_{i+1}$ and spectral $band_i$.

- VIs related to leaf pigments or cell structure ('leaf pigment and canopy density indices'),
- VIs related to water content ('water stress indices'),
- VIs designed to parameterize the shape of the recorded spectra ('angle indices'), and
- VIs looking specifically at the red edge of vegetation spectra ('red edge indices').

2.5. Class separability and classification: T-test and Random Forest classifier

For assessing the separability of the two groups of ring-barked and control trees, a modified statistical t-test (Welch-test) was utilized. In this respect, VIs, REIPs and angel indices of the two groups for each date were statistically examined.

To further examine the separability of control and ring-barked trees, we also used a classical Random Forest classifier (Breiman, 2001). This allowed to examine the individual features for their respective discriminative power, as well as to 1) examine which input data is best suitable to distinguish stressed and unstressed trees, and 2) to determine the time at which differences between the spectra of the two groups (ring-barked trees and control trees) are at first recognizable. All features were tested to determine the highest importance for separating the two vitality levels/groups by using feature importance measures in Random Forest.(all individual bands, VIs, REIPs, angle indices, and derivatives).

.The Random Forest classifications were applied in R Version 3.4 (R Core Team, 2017) using the randomForest (Liaw and Wiener, 2002) package. The models were trained with the often used standard values for mtry (square root of the number of input data) and 1000 trees (Immitzer et al., 2019, 2018).

3. Results

3.1. General reactions of the two forest stands to the artificial stress

Although the two forest stands grow under very similar site conditions, they reacted differently to ring-barking. The younger, well-maintained forest stand ($Stand_{young}$) was found less susceptibility to the artificial stress, compared to the older, denser forest stand ($Stand_{old}$), where trees are planted irregularly.

Within the first growing season (2013), no significant changes of the stressed trees could be detected during field surveys. Only in a few sampled trees a slightly higher loss of needles was recorded, especially concerning the needles from older age classes. All monitored trees were nevertheless able to withstand the artificially induced stress for almost a year. Eleven months after ring-barking, the crown condition assessment on 22 May 2014, showed only minor changes in yellowing, fructification and needle loss. During the last two assessments in June 2014 bark beetle attacks could be detected in several trees (see dark blue line in Fig. 5).

Tree climbers detected a bark beetle attack in two ring-barked tree tops during needle sampling (05 June 2014) in $Stand_{old}$. The infestation was not visible from the ground, also no boring dust was visible on the tree foot. During the last two field surveys (13 and 18 June 2014) bark beetle infestations were found in several, predominantly ring-barked trees in both forest stands: 49 trees in $Stand_{old}$ and 35 trees in $Stand_{young}$ (see Table 3). Only four control trees were infested in the older forest stand ($Stand_{old}$) and two control trees were infested in the younger forest stand ($Stand_{young}$). In both forest stands, needle loss increased significantly between the last two field assessments (13 and 18 June 2014) for the ring-barked trees. For some of these trees with minor needle loss, it was assumed that the bark beetles just recently drilled into the trees. The infestation led to the end of the experiment, as all infested trees had to be removed to secure the remaining forest.

3.2. Changes of needle and tree crown spectra between start and end of experiment

To localize changes in both needle and tree crown spectra over time, the mean spectra of ring-barked trees and mean control trees (± standard deviation) were examined (Fig. 6). The graphs on the left show a significant change in vitality of the needle spectra (needle year 2010) of the older forest stand ($Stand_{old}$). At the time of the first sampling (16 July 2013, Fig. 6a), the averaged spectra of the control trees and the stressed trees were almost alike. At the last sampling date (23 June

Table 3
Overview of temporal development of bark beetle infestation in Einsiedl ($Stand_{old}$) and Gaderbogen ($Stand_{young}$) in 2014 during field assessment.

Date	$Stand_{old}$		$Stand_{young}$	
	Attacked ring-barked trees	Attacked control trees	Attacked ring-barked trees	Attacked control trees
10.01.2014	0	0	0	0
25.02.2014	0	0	0	0
27.03.2014	0	0	0	0
11.04.2014	0	0	0	0
22.05.2014	0	0	0	0
14.06.2014	40	4	28	0
17.06.2014	49	4	35	2

Data from 2013 are not shown since there were no infestations recorded.

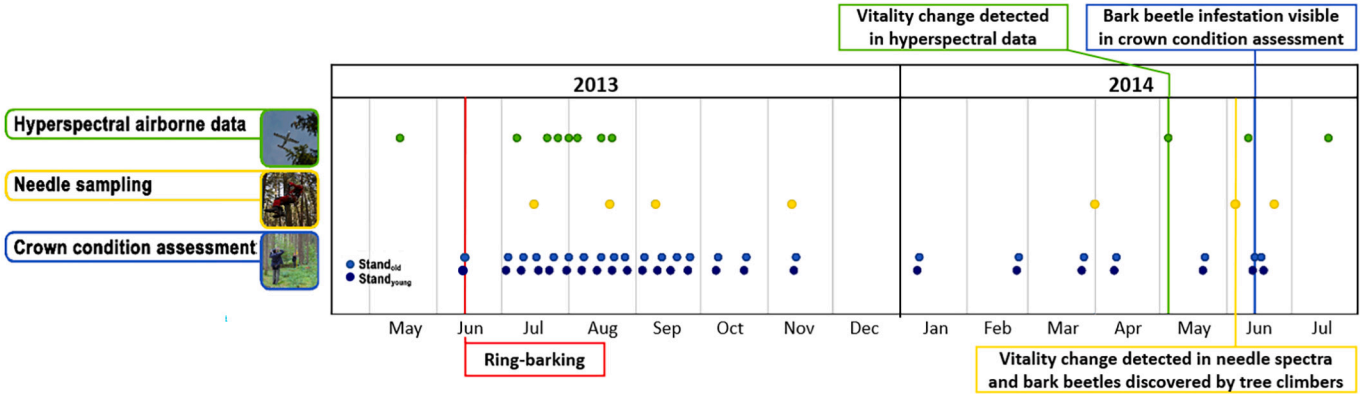

Fig. 5. Overview of data acquisitions from airborne platform and field activities. The vertical lines indicate important dates: ring-barking (red), vitality change detected in needle spectra (yellow), vitality change detected in the hyperspectral airborne data (green) as well as bark beetle infestation visible in the field (dark blue). (For interpretation of the references to colour in this figure legend, the reader is referred to the web version of this article.)

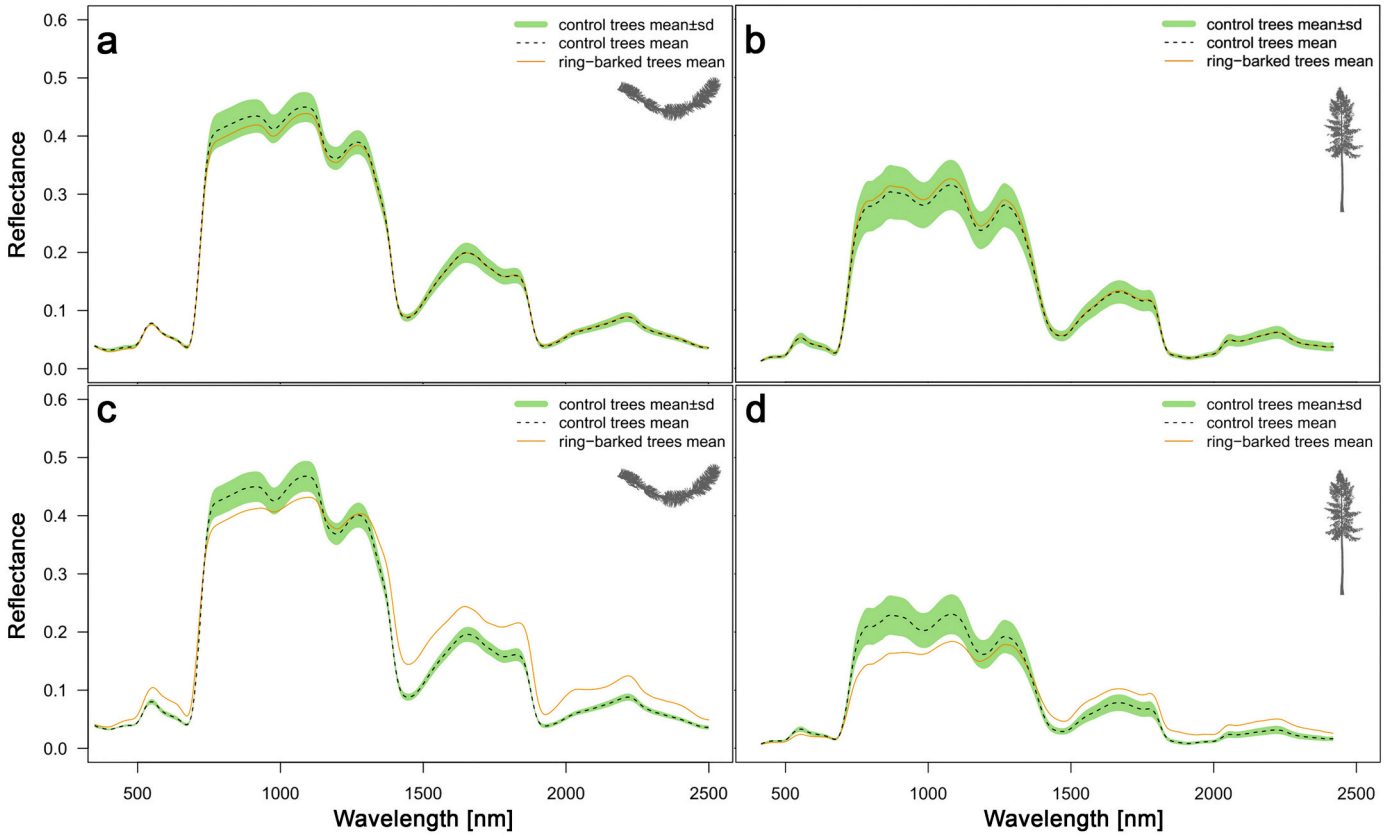

Fig. 6. Mean spectral signature of needles (left) and mean spectral signature of tree crowns (right) of the forest $Stand_{old}$: spectral signatures of the needle year 2010 from 16.07.2013 (a) and 23.06.2014 (c) and spectral crown signatures from 15.05.2013 (b) and 18.07.2013 (d).

2014, Fig. 6c), however, the spectra of stressed trees differed significantly from the mean of the control trees, while the control tree spectra had not changed over time. Compared to the mean of the control trees, the needle reflectance of artificially stressed trees increased in the visible (mainly red) and SWIR range, while a decrease was observed in the NIR. This is a typical reaction to vitality losses where contents of photosynthetic pigments (i.e. chlorophyll) and leaf water are reduced, while the cell structure is altered (Carter and Knapp, 2001; Entcheva Campbell et al., 2004; Meiforth et al., 2020).

The crown spectra behaved in a similar way (Fig. 6b,d). At the beginning of the experiment (15 May 2013, Fig. 6b) the spectra of ring-barked trees and the control group are very similar while changes between the two groups are clearly visible 14 month later (18 July 2014, Fig. 6d). The spectral reflectance decreased both in the visible and NIR and increased in SWIR range. Hence, in addition to altered leaf optical properties, a needle loss is evident from those spectra.

These stress-induced changes were mainly visible in the older forest stand ($Stand_{old}$), whereas in the well-maintained younger forest stand ($Stand_{young}$) only minor changes were observed (not shown).

3.3. Temporal changes of spectral features

3.3.1. Derivatives and red edge parameters

The derivative analysis and the two red edge parameters show similar results for needle and tree crown data (Figs. 7 and 8). For the needle spectra, needle year 2010 of the older forest stand is displayed as example (Fig. 7). When comparing the mean control spectra (Fig. 7a,c) with the mean spectra of the ring-barked trees (Fig. 7b,d), the spectra of the two groups are very similar at the beginning of the measurement campaign (16 July 2013). Likewise, the green peak and the $REIP_{FDR}$ have similar values. At the end of the measurement campaign, however, there is a clear difference between the two groups. The averaged spectrum of the control trees is almost unchanged, while the spectrum of the stressed trees has changed. We notice that the green peak has moved from 550 to 554 nm while the $REIP_{FDR}$ has decreased from 719 to 712 nm. The same behavior is observable for the other needle age classes (not shown) of $Stand_{old}$, whereas the changes are less distinct in the younger forest stand $Stand_{young}$ (not shown).

The hyperspectral tree crown data display a similar trend (Fig. 8). As an example, the spectra and derivates of a ring-barked tree are plotted (tree no. 81, Fig. 8b and d). This tree was infested by bark beetles in 2014. The green peak shifted from 556.1 to 563.3 nm, while the $REIP_{FDR}$ decreased from 721.7 to 714.5 nm. Whereas the spectra of a control tree (tree no. 87) from the same stand (Fig. 8a and c) shows only small changes in spectral reflectance. Green peak and $REIP_{FDR}$ do not change.

The needle spectra of this tree, as well as REIPs, change in a similar way (Fig. 9). Shown is the first sample of 2013 together with three sampling dates of the second vegetation period. Both $REIP_{FDR}$ (grey) and $REIP_{Guyot}$ (red) decrease continually over time, with $REIP_{FRD}$ revealing a slightly stronger decrease.

Bean plots of the pooled data combining observations from all trees and the two test sites, show the temporal development of the $REIP_{Guyot}$ values for both needle (Fig. 10) and tree crown spectra (Fig. 11). Even if the sample size for the needle spectra is small, the temporal development of both needle spectra and tree crown spectra is shown with bean plots for better visual comparison. For the needle data of $Stand_{old}$ (Fig. 10a), the $REIP_{Guyot}$ values for the stressed trees (orange) decrease from 01 April 2014 onwards for all needle age classes (only needle age class 2013 shown in Fig. 10), while the control trees (green) remain constant or experience a slight increase. For the needles of $Stand_{young}$ (Fig. 10b), the two groups are significantly different from 05 June 2014 onwards.

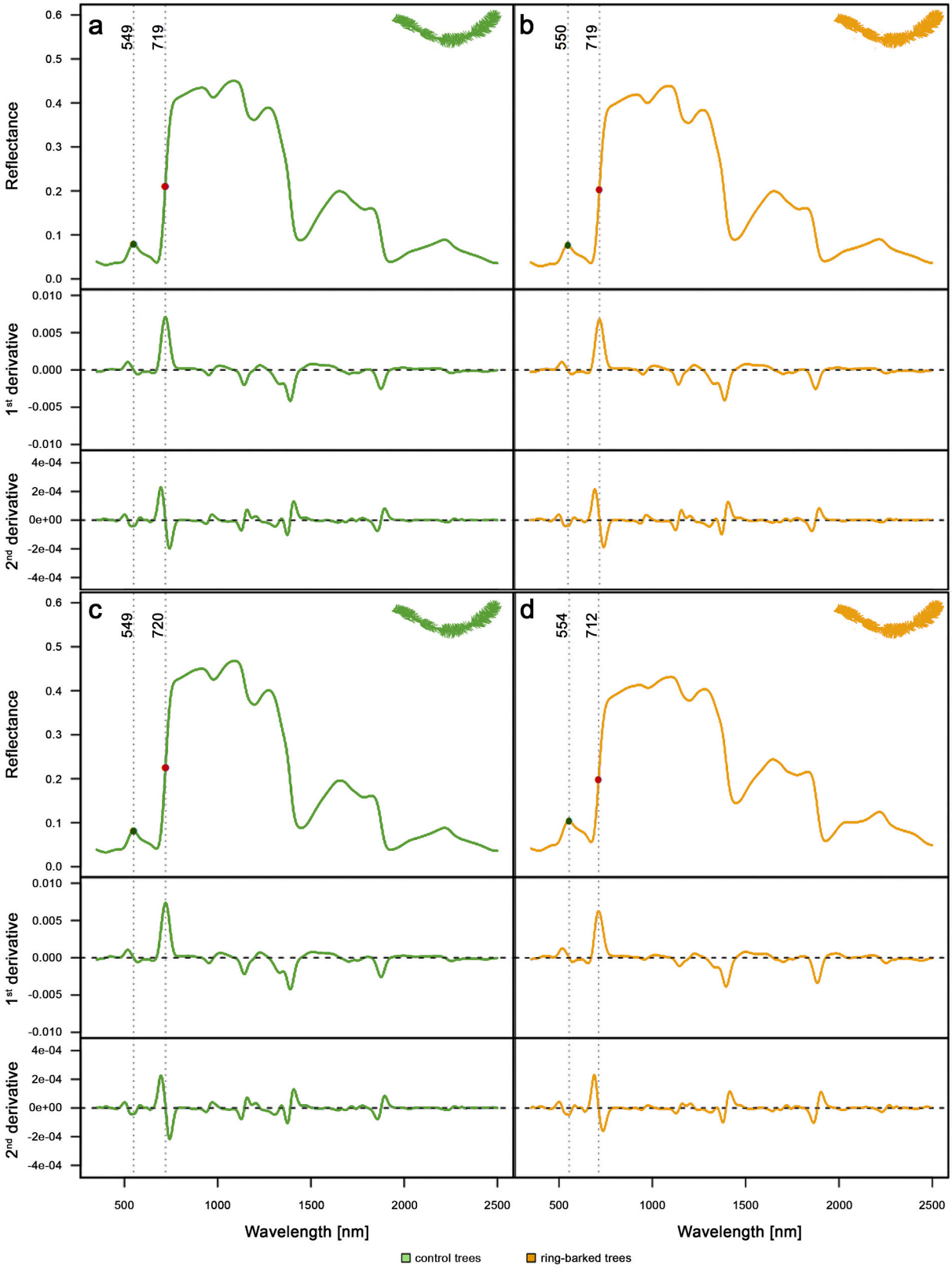

Fig. 7. Mean needle spectra (needle year 2010) of the forest $Stand_{old}$ with 1st and 2nd derivative of control trees (left) and ring-barked trees (right) from 16.07.2013 (a, b) and 23.06.2014 (c, d). The green and red dots indicate the location of green peak and $REIP_{FDR}$. (For interpretation of the references to colour in this figure legend, the reader is referred to the web version of this article.)

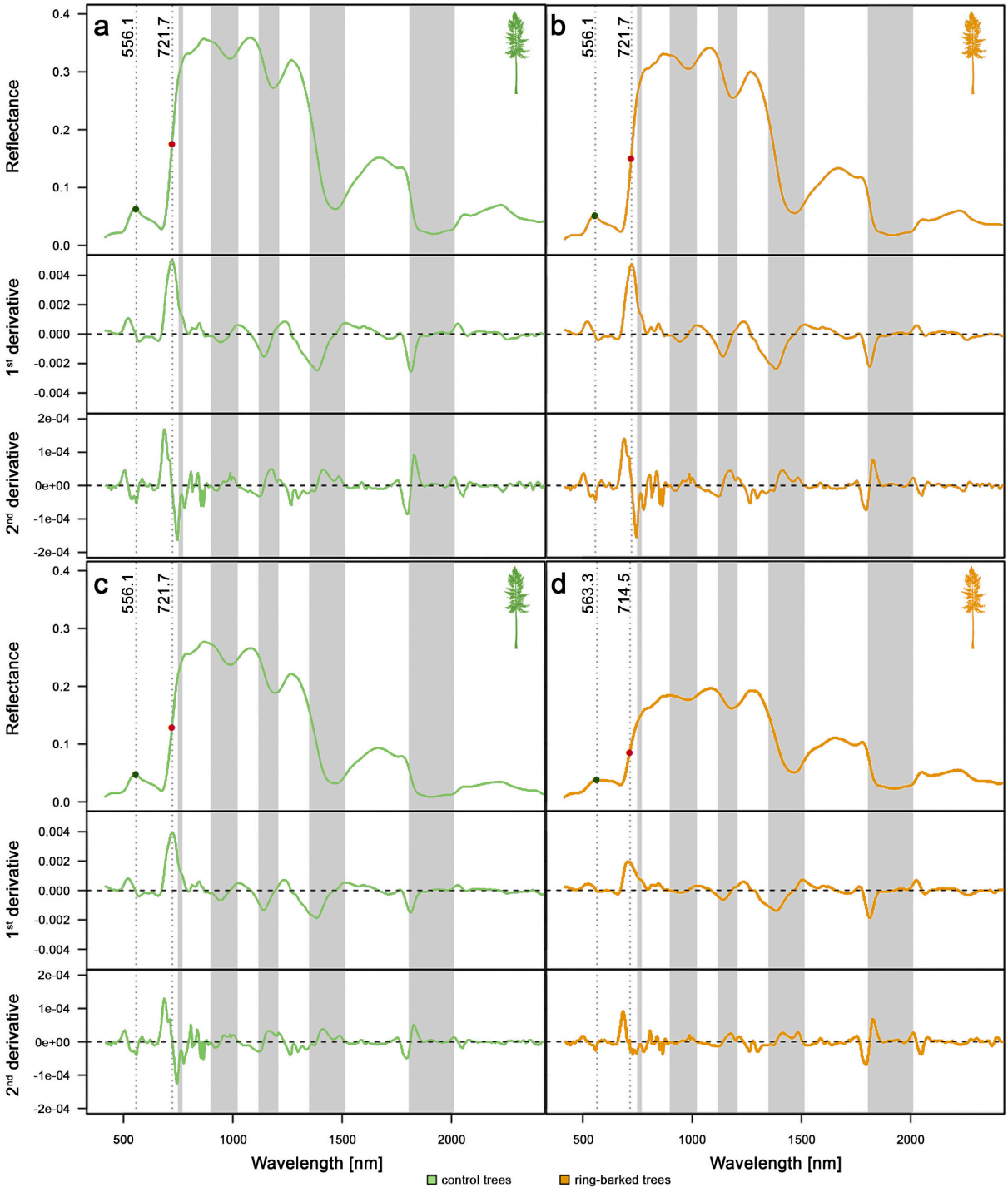

Fig. 8. Tree crown spectra of a ring-barked tree in $Stand_{old}$ (tree no. 81, right) and a control tree (tree no. 87, left) with 1st and 2nd derivative from 15.05.2013 (a, b) and 11.06.2014 (c, d). Also shown are the location of green peak (green dot) and $REIP_{FDR}$ (red dot). The grey areas represent those areas that were interpolated in the preprocessing due to gaseous absorptions in the atmosphere (O_3, H_2O, CO_2). (For interpretation of the references to colour in this figure legend, the reader is referred to the web version of this article.)

The $REIP_{Guyot}$ values for the tree crown spectra behave similarly (Fig. 11). In 2013, the two groups show comparable values and remain nearly unchanged during the first vegetation period. From May 2014 onwards the two groups differ, especially in the older forest stand ($Stand_{old}$, Fig. 11a). Note that the apparent separability of the two groups in $Stand_{young}$ (Fig. 11b) on 21 August 2013 are artefacts, due to cloud shadows in the HySpex data over that area.

3.3.2. *Vegetation indices*

Analyzing the various VIs (Table 2), we found that the water stress indices generally react less clearly to the artificial weakening, whereas the leaf pigment and cell structure indices respond stronger.

For the needle analysis of the older forest stand ($Stand_{old}$) most of the VIs (GI, PRI, MCARI, MRESR, MSI, NDII, NDLI, NDWI, RENDVI and WBI) show significant difference towards the end of the study period (last two measurements 04 and 23 June 2014). However, the VIs vary

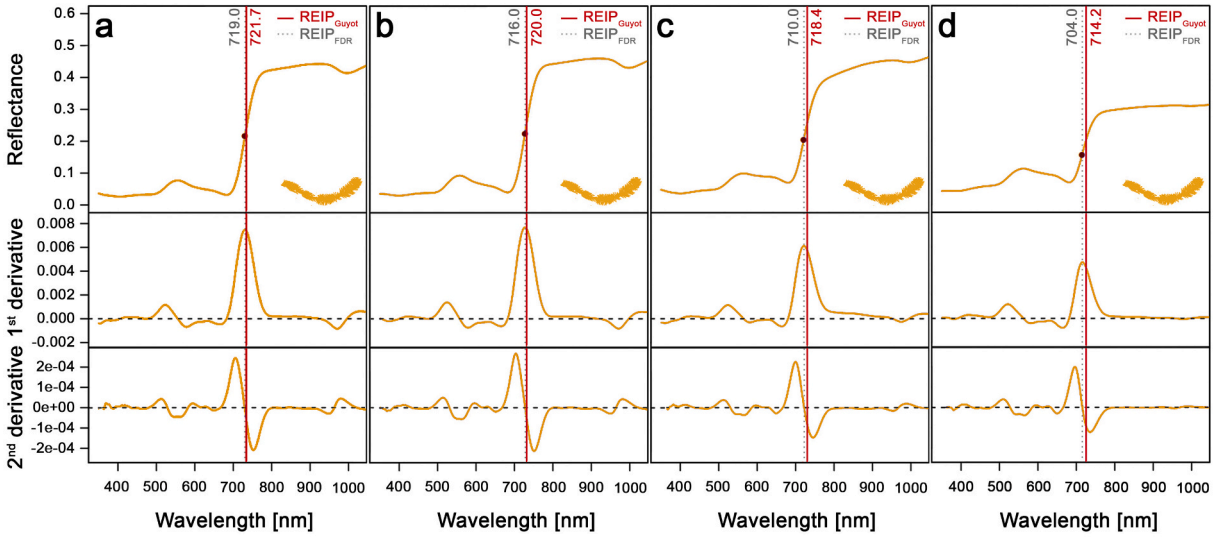

Fig. 9. Temporal development of needle reflectance spectra, 1st and 2nd derivative and two inflection points of a ring-barked tree in $Stand_{old}$ (tree no. 54 - needle year 2010): $REIP_{FDR}$ of the first derivate (grey) and $REIP_{Guyot}$ (red) for 16.07.2013 (a), 01.04.2014 (b), 05.06.2014 (c) and 23.06.2014 (d). (For interpretation of the references to colour in this figure legend, the reader is referred to the web version of this article.)

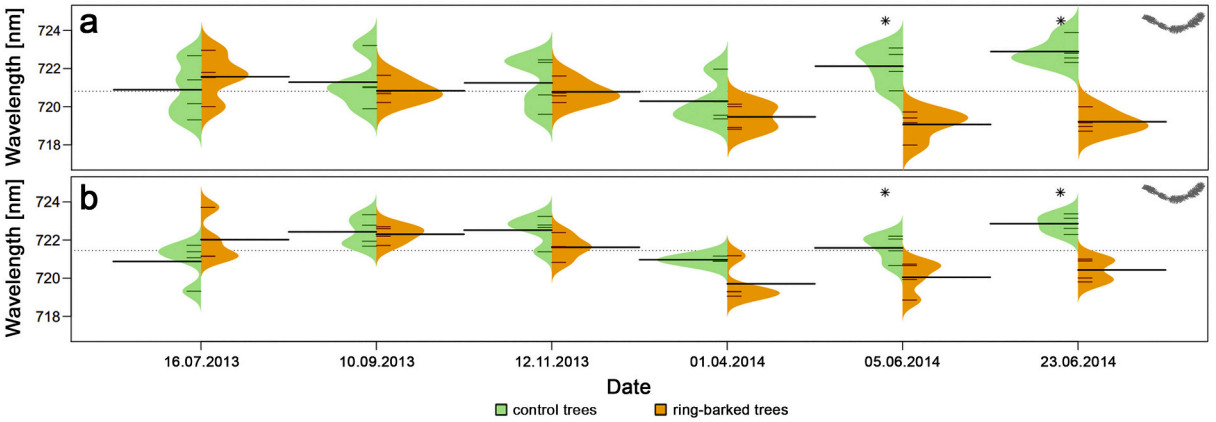

Fig. 10. Development of $REIP_{Guyot}$ derived from needle spectra (needle year 2013) of control trees (green) and ring-barked trees (orange) $Stand_{old}$ (a) and $Stand_{young}$ (b). In a single bean, the short horizontal lines represent measured values. The black thick lines are the means of the particular group. The symbol * indicates statistically significant differences. Note: The sample size of needle spectra (2 × 8) is small for bean plots but they are used for an easy visual comparison with the bean plots of the tree crown spectra. (For interpretation of the references to colour in this figure legend, the reader is referred to the web version of this article.)

slightly within the different needle years. For the younger forest stand ($Stand_{young}$) the two groups are significantly different starting from 05 June 2014 for GI, MCARI and MRESER. Again, some variations between needle classes are seen. In some cases, the VIs are only significantly different for the last measurement date (23 June 2014).

The two most reactive indices PRI and MCARI are shown as bean plots for both forest stands (Fig. 12). The PRI values of the stressed trees are steadily decreasing in 2014. For the needle years 2013 and 2012, this is significant as of 05 June 2014 in $Stand_{old}$ (Fig. 12). The PRI of $Stand_{young}$ does show similar changes without being significant.

For $Stand_{old}$ the mean values of the ring-barked trees increase for MCARI in both forest stands from 01 April 2014 onwards. The two groups show a significant change for the younger needle years (2013 and 2012) starting from 05 June 2014. The same development was found for the needle spectra in $Stand_{young}$.

Similarly, the tree crown spectra showed changes between the control and ring-barked trees over time using the leaf pigment and canopy density indices (GI, MCARI, MRESR, PRI, PRSI and RENDVI). The results for PSRI and MRESR are shown as example (Figs. 13 and 14). From the first measurement in the second vegetation period (05 May 2014) onwards, all these indices were significantly different for the two groups for the older forest stand. On the contrary, for the younger forest stand, only the PRI values showed a significant reaction. For the other indices in $Stand_{young}$ the difference between the two groups appeared first at 11 June 2014.

For the needle spectra, only the SASI shows significant differences between the ring-barked trees and the control trees (Fig. 15), whereas ANIR is insignificant. The SASI mean values differ significantly in $Stand_{old}$ starting at 05 June 2014 for needle age class 2013 (Fig. 15a), for the needle age classes 2010–2012 starting from 23 June 2014 (not shown). In $Stand_{young}$, there are significant differences between the two groups, but less uniform than in $Stand_{old}$. However, a constant, significant change is seen in needle year 2013 from 05 June 2014 onwards (Fig. 15b).

The temporal development of the angle indices for the tree crown spectra is in comparison to the needle spectra for both forests stands and both angle indices (SASI and ANIR) equivalent. The two tree groups differ from 06 November 2014 for both angle indices in $Stand_{old}$, whereas no significant difference can be seen in $Stand_{young}$. The temporal evolution of SASI is shown in Fig. 16.

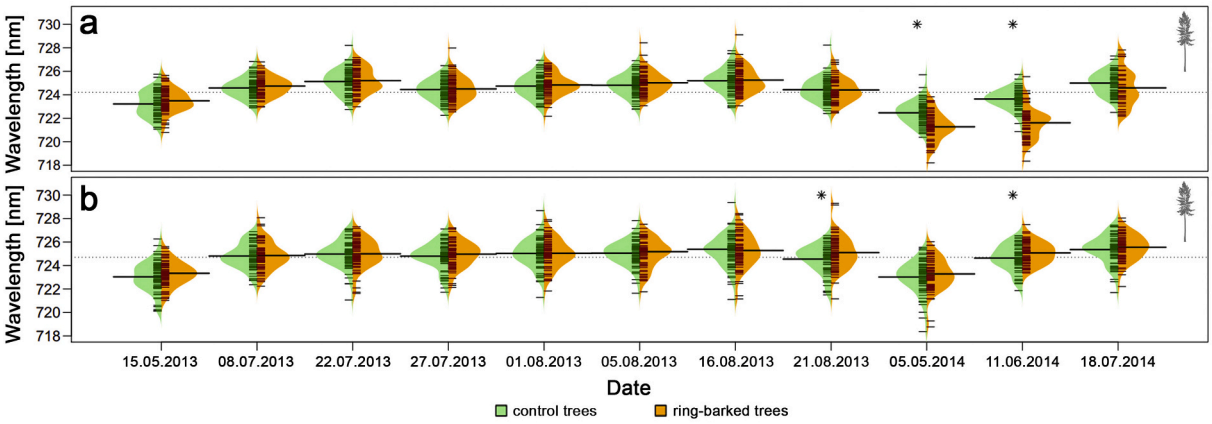

Fig. 11. Development of Red Edge Inflection Point ($REIP_{Guyot}$) derived from tree crown spectra of control trees (green) and ring-barked trees (orange) as a function of time for $Stand_{old}$ (a) and $Stand_{young}$ (b). The symbol * indicates statistically significant differences. Note: At the last acquisition date (18 July 2014) infested trees have already been removed from the forest stands, therefor the change between the two groups is not significant any more. (For interpretation of the references to colour in this figure legend, the reader is referred to the web version of this article.)

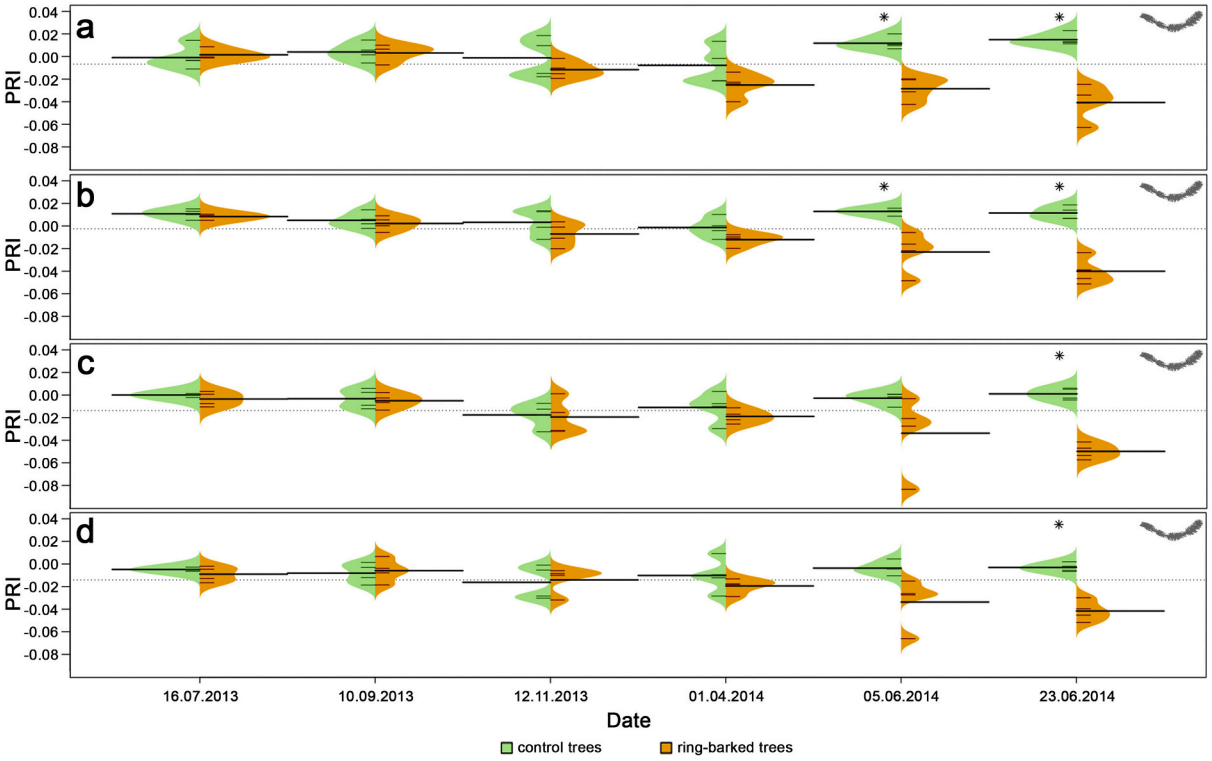

Fig. 12. Development of Photochemical Reflectance Index (PRI) of control trees (green) and ring-barked trees (orange) for needle spectra over time in $Stand_{old}$ separated for the needle years 2013 (a), 2012 (b), 2011 (c) and 2010 (d). The symbol * indicates statistically significant differences. Note: The sample size of needle spectra (2 × 8) is small for bean plots but they are used for an easy visual comparison with the bean plots of the tree crown spectra. (For interpretation of the references to colour in this figure legend, the reader is referred to the web version of this article.)

3.4. Feature importance for vitality loss detection (Random Forest)

The Random Forest (RF) classification algorithm was applied separately for the two forests, the spectra of single needle age classes (Table 4) and the tree crown spectra (Table 5), respectively. For the classification, the individual spectra and their first and second derivatives, and all VIs were used. The overall accuracy and the kappa index were calculated to validate the classification.

In both forests stands the needle spectra of the two groups could not be separated in the first vegetation period (2013). In the second year, the two tree groups could be separated for needle age classes 2013, 2012 and 2010 for both forest stands with 75% overall accuracy at 05 June 2014. For all needle age classes in both forest stands the two groups are discriminable with a high accuracy (88%) and a high kappa coefficient (0.75) at the last sampling date (23 June 2014). In most cases, the spectra or the first or second derivative were chosen as the best variables for separating the two groups, over the VIs or angle indices.

Whereas for the needle spectra only a few measurements were available, a large amount of airborne data could be used for the tree crown analysis: for each forest stand, 70 ring-barked trees and 70 control

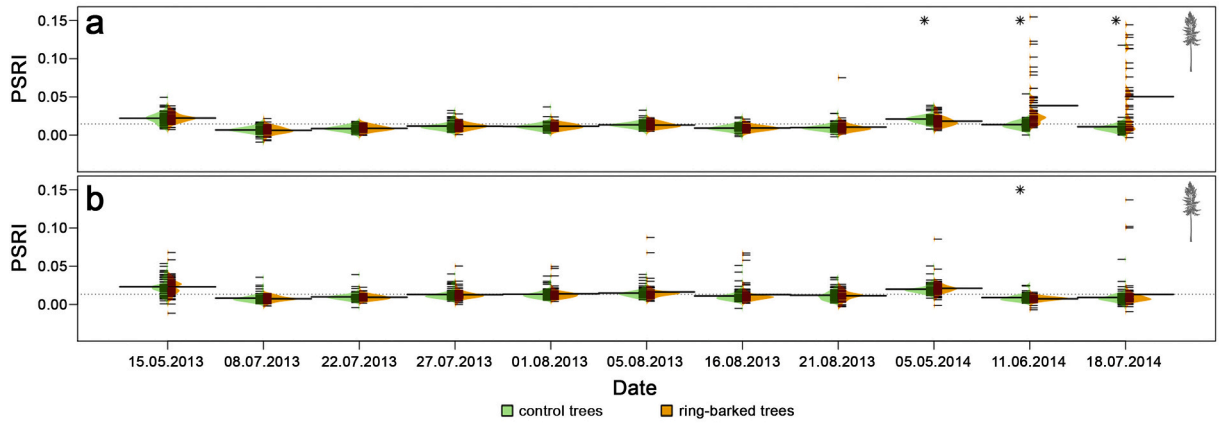

Fig. 13. Development of Plant Senescence Reflectance Index (PSRI) of control trees (green) and ring-barked trees (orange) for tree crown spectra over time for $Stand_{old}$ (a) and $Stand_{young}$ (b). The symbol * indicates statistically significant differences. Note: At the last acquisition date (18 July 2014) infested trees have already been removed from the forest stands, therefor the change between the two groups is not significant any more for the $Stand_{young}$. (For interpretation of the references to colour in this figure legend, the reader is referred to the web version of this article.)

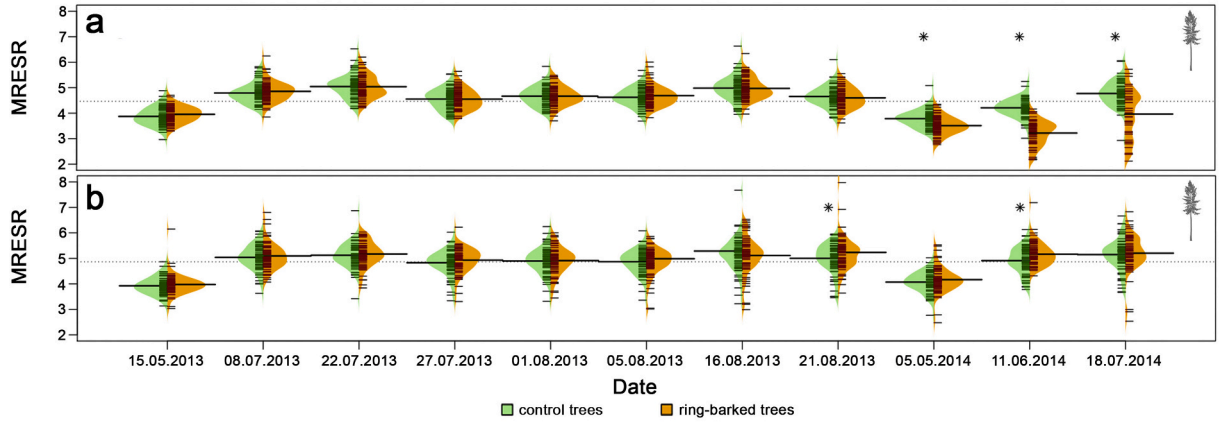

Fig. 14. Development of Modified Red Edge Simple Ratio (MRESR) of control trees (green) and ring-barked trees (orange) for tree crown spectra over time for $Stand_{old}$ (a) and $Stand_{young}$ (b). The symbol * indicates statistically significant differences. Note: At the last acquisition date (18 July 2014) infested trees have already been removed from the forest stands, therefor the change between the two groups is not significant any more for the $Stand_{young}$. (For interpretation of the references to colour in this figure legend, the reader is referred to the web version of this article.)

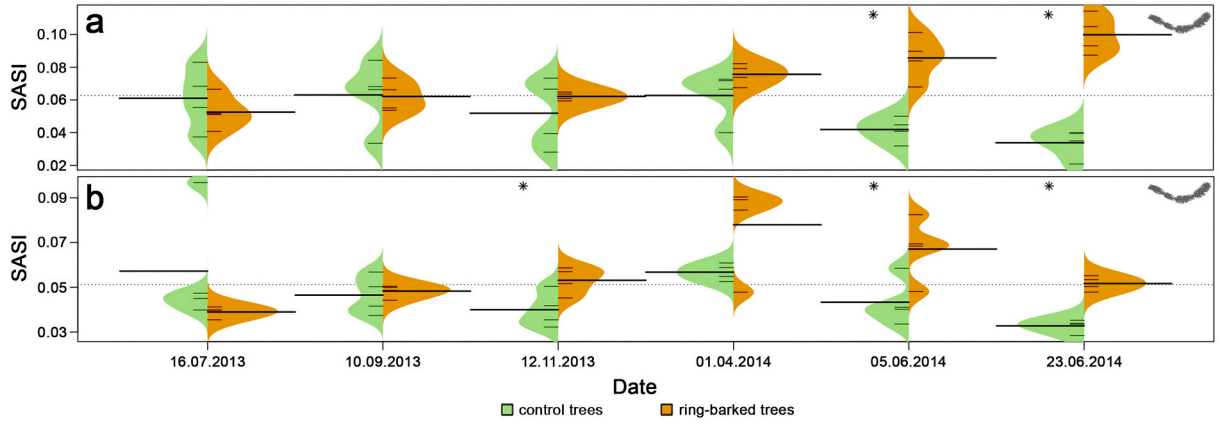

Fig. 15. Development of Shortwave Angle Slope Index (SASI) of control trees (green) and ring-barked trees (orange) for needle spectra (needle year 2013) in $Stand_{old}$ (a) and $Stand_{young}$ (b). The symbol * indicates statistically significant differences. Note: The sample size of needle spectra (2 × 8) is small for bean plots but they are used for an easy visual comparison with the bean plots of the tree crown spectra. (For interpretation of the references to colour in this figure legend, the reader is referred to the web version of this article.)

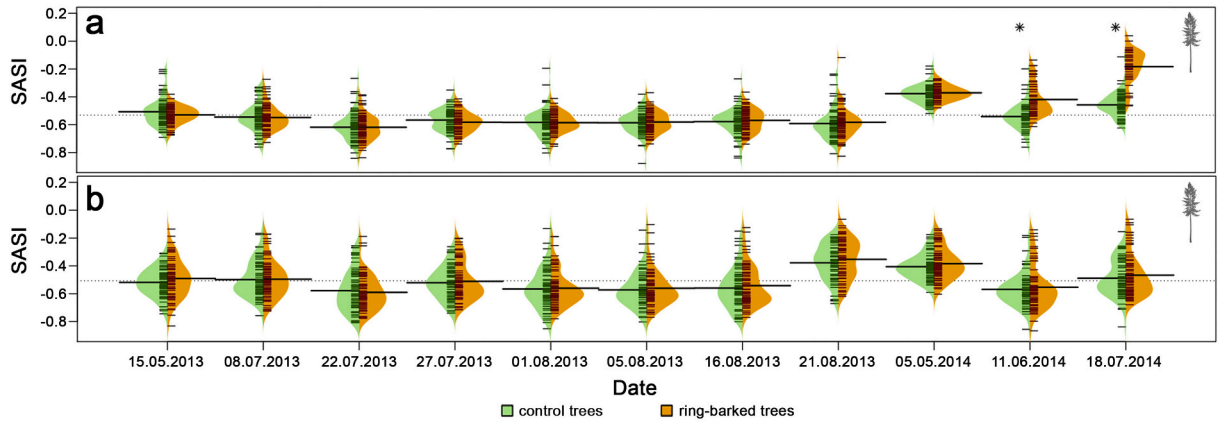

Fig. 16. Development of Shortwave Angle Slope Index (SASI) of control trees (green) and ring-barked trees (orange) for tree crown spectra for $Stand_{old}$ (a) and $Stand_{young}$ (b). The symbol * indicates statistically significant differences. Note: At the last acquisition date (18 July 2014) infested trees have already been removed from the forest stands. (For interpretation of the references to colour in this figure legend, the reader is referred to the web version of this article.)

Table 4
Overall accuracy and kappa coefficient values of the Random Forest classification for the four needle classes (2013−2010) for $Stand_{old}$ (Einsiedl) and $Stand_{young}$ (Gaderbogen).

	Date	Needle year 2013		Needle year 2012		Needle year 2011		Needle year 2010	
		Accuracy	Kappa	Accuracy	Kappa	Accuracy	Kappa	Accuracy	Kappa
$Stand_{old}$	16.07.2013	0.25	−0.50	0.00	−1.00	0.50	0.00	0.13	−0.75
	20.08.2013	0.25	−0.50	0.25	−0.50	0.13	−0.75	0.38	−0.25
	10.09.2013	0.25	−0.50	0.38	−0.25	0.63	0.25	0.13	−0.75
	12.11.2013	0.38	−0.25	0.38	−0.25	0.25	−0.50	0.38	−0.25
	01.04.2014	0.38	−0.25	0.25	−0.50	0.50	0.00	0.00	−1.00
	05.06.2014	0.75	0.50	0.75	0.50	0.63	0.25	0.75	0.50
	23.06.2014	0.88	0.75	0.88	0.75	0.88	0.75	0.88	0.75
$Stand_{young}$	16.07.2013	0.25	−0.50	0.00	−1.00	0.50	0.00	0.00	−1.00
	20.08.2013	0.25	−0.50	0.25	−0.50	0.13	−0.75	0.50	0.00
	10.09.2013	0.25	−0.50	0.38	−0.25	0.63	0.25	0.13	−0.75
	12.11.2013	0.25	−0.50	0.38	−0.25	0.25	−0.50	0.38	−0.25
	01.04.2014	0.38	−0.25	0.50	0.00	0.63	0.25	0.00	−1.00
	05.06.2014	0.75	0.50	0.75	0.50	0.38	−0.25	0.75	0.50
	23.06.2014	0.88	0.75	0.88	0.75	0.88	0.75	0.88	0.75

Nobs = 2 × 8.

Table 5
Overall accuracy and kappa coefficient values of the Random Forest classification for the tree crown spectra for $Stand_{old}$ (Einsiedl) and $Stand_{young}$ (Gaderbogen).

	$Stand_{old}$		**$Stand_{young}$**	
Date	Accuracy	Kappa	Accuracy	Kappa
15.05.2013	0.56	0.11	0.52	0.04
08.07.2013	0.56	0.12	0.55	0.10
22.07.2013	0.50	0.00	0.44	-0.13
27.07.2013	0.43	-0.13	0.54	0.07
01.08.2013	0.56	0.11	0.41	-0.17
05.08.2013	0.51	0.03	0.55	0.10
16.08.2013	0.49	-0.01	0.43	-0.14
21.08.2013	0.55	0.10	0.54	0.07
05.05.2014	0.79	0.58	0.51	0.03
11.06.2014	0.92	0.84	0.58	0.16
18.07.2014	0.94	0.88	0.50	0.00

The last row is marked grey, since at that date (18 July 2014) some infested trees were already removed. Nobs = 2 × 140.

trees were available. In the first vegetation season (2013), in both forest stands the ring-barked trees and control trees could not be separated. At the beginning of the second vegetation season (05 May 2014), however, the two groups were distinct separable with 79% overall accuracy and a kappa coefficient of 0.58 in the older forest stand ($Stand_{old}$); 1 month later (11 June 2014) even with 92% accuracy. On the contrary, in $Stand_{young}$ the two groups could not be separated clearly.

The best performing features for needle spectra were the 1st and 2nd derivatives, followed by spectral bands. In contrary to the needle spectra some VIs were also chosen as best performing variables. For $Stand_{old}$ PRI and WBI (WBI only for the last date) showed best results, whereas for forest $Stand_{young}$ MRESR was chosen.

4. Discussion

The study showed that vitality changes in Norway spruce forests can be reliably detected with hyperspectral remote sensing data. Most importantly, the stressed and control trees could be distinguished by airborne data earlier, then by field observations from the ground.

4.1. Detection of spectral changes with remote sensing data

The manually induced stress (ring-barking) did only show noticeable changes after nearly 1 year. In the first vegetation period, the crown condition assessments as well as remote sensing data did hardly show any changes. Only during needle sampling a higher needle loss of the stressed trees was detectable, mainly for the older needle age classes. In the second vegetation period, however, the stressed trees of the older forest stand had an increased susceptibility to bark beetle infestation. Those trees often showed changes in their spectral behavior. The spectral response of stressed trees could be seen in both needle and tree crown hyperspectral data, and this well before changes in the field were visible. The largest change was found in ring-barked trees with additional bark beetle infestation. To what extent the detected changes are connected to the additional bark beetle infestation or whether the higher susceptibility is due to the artificial weakening, must be examined further. Answering this question is of high importance with respect to the detection of the “green attack” stadium (Abdullah et al., 2018; Meddens et al., 2011; Wulder et al., 2006).

Please note that these results do not fully coincide with the publication of the first results of the needle spectra analysis of the same experiment in Reichmuth et al. (2018). However, it should be noted that there are some methodological errors and misinterpretations in the mentioned paper. Therefor we would like to set some of its content and methodological description right, for example, the number of test trees is incorrect and the measurement method is inaccurately described. We want to make clear, that the bark beetle infestation in the test site was first discovered by the tree climber and some of the authors during the needle sampling on 5 June 2014.

We found rather strong differences between the young and old stands, with the older stand reacting stronger to the stress. In the younger forest stand ($Stand_{young}$) we found only minor detectable differences between the two groups. This might be due to a higher vitality of the younger trees (Moore, 2013), which are not as easily harmed by ring-barking compared to the older spruce stand.

Even if it was clearly possible to differentiate the two groups in the second vegetation period with the tested approaches, it should be kept in mind that the early determination of the tree vitality is a very complex topic influenced by many factors (site characteristics, water supply, severity and type of injury). During the same period (2013–14) ring-barked Scot pine trees in Czech Republic survived also for 2 years after stem girdling (Fajstavr et al., 2017). In addition, trees may show different signs of damage due to their current (vitality) status and the comparability between ring-barking and a bark beetle infestation is difficult to discriminate. Moreover, trees (even of a given species and growth stadium) show a large natural variability, as can be demonstrated both experimentally (Andreu et al., 2007; McElhinny et al., 2005; Ratcliffe et al., 2015; Rautiainen et al., 2018) and using physically based radiative transfer models (Rautiainen et al., 2004; Schlerf and Atzberger, 2006).

4.2. Most discriminative features for separating stressed and healthy trees

For separating the two groups (stressed and healthy trees) a large variety of features were tested including spectra, derivates, classical VIs, angle indices and red edge parameters. The measured healthy and stressed spruce spectral signatures match related studies (Abdullah et al., 2018; Brovkina et al., 2017; Foster et al., 2017). Changes in needle and tree crown hyperspectral signatures were detectable in the older spruce stand, in particular in VIS, red-edge region and SWIR. This finding is in line with other studies of spruce. Abdullah et al. (2019) investigated the early-stress detection induced by bark beetles. Reflectance changes of infested Norway spruce trees were observable especially in the red-edge and shortwave infrared regions both for leaf and canopy levels. Entcheva Campbell et al. (2004) detected initial damage using hyperspectral airborne data in the red-edge region (673–724 nm) showing maximum sensitivity to the beginning damage. Foster et al. (2017) examined early-stage bark beetle infestation in Engelman spruce. They particularly found the SWIR region important.

In our study, especially derivatives and REIP contained valuable information to separate the two groups. On the contrary, for the younger stand, only minor changes were observed.

The analysis of the needle spectra revealed clear differences between the two groups. The temporal changes could be seen in the derivatives and derivable measures, like green peak and REIP. The green peak shifted to higher wavelength (from 556 to 638 nm), while the REIPs moved to shorter wavelength with increasing stress. The shift to shorter wavelength ranges is referred to as ‘blue shift’ (Slonecker, 2011) and a clear stress indicator as it indicates a loss of chlorophyll and leaf area (Carter, 1994; Rock et al., 1988).

Besides the derivatives, several (classical) VIs were relevant to separate the two groups for needle spectra. Good separations were possible using for example the Photochemical Reflectance Index (PRI) and Modified Chlorophyll Absorption Ratio Index (MCARI). For the last two samplings the older forest stand showed significant differences between the groups, but the separability also emerged in earlier samplings. For needle spectra, the angle index SASI was also a helpful feature, whereas with the second tested angle index, ANIR, the two groups could not be separated.

Regarding the crown spectra, the two groups could be differentiated in the older forest stand beginning from May 2014 (12 months after the ring-barking) – at a time very similar to the leaf level analysis. The spectral signatures of the ring-barked trees had lower reflectance values compared to the healthy trees. Like for the needle spectra, REIP was a valuable measure to differentiate the two groups. Also, green peak values shifted to longer wavelength over time, whereas REIP values shifted to shorter wavelength. For the tree spectra, the following VIs were most suitable to differentiate the two groups: GI, MRESR, PSRI and RENDVI. Both angle indices, ANIR and SASI, were able to detect a change of the ring-barked group in the older forest stand.

The RF classification models confirmed the separability of the two groups in the second vegetation period. The needle spectra had a high overall accuracy (75–88%), but it must be noted that for the needle analysis only a small sample size was at hand due to the costly and complex needle sampling (for each forest stand, only four ring-barked trees and four control trees were probed). The spectra or the first or second derivative were chosen as the best variables for separating the two groups. For a future study, however, a higher sample size would be advantageous.

For the old forest stand ($Stand_{old}$, see Table 5) but not the younger stand, the tree crown spectra of the two groups spectra could be separated by the RF classifier with a 79% overall accuracy at the beginning of

the second vegetation period and 1 month later with 92% overall accuracy. The first or second derivative were chosen as the best variables for separating the two groups followed by the spectra, nearly outperforming all VIs (expect PRI, WBI and MRESR) including the angle indices and REIP.

4.3. Application scenarios

The unexpectedly late reaction of the spruce trees to ring-barking made it necessary to extent the time span of the experiment from one to two growing seasons. This unforeseen development led on the other hand to several additional hyperspectral overflights, creating a scientific revealing/valuable data set. For practical commercial applications, however, such dense airborne data acquisitions are probably too costly. Further, in commercial forestry, timing matters to detect weakened trees, which should be removed immediately. Probably, only a spaceborne (with high and regular revisit frequency) imaging spectrometer with high spatial resolution would be cost-effective. Further in commercial forestry, timing matters to detect weakened trees. It should be noted, that our analyses were all done retrospectively. For a practicable implementation the vitality change recognition would have to be done with one overflight, whereby the determination of the optimum date remains a challenge. Currently, for a regular monitoring, and due to cost reasons/restraints, only freely available multi-spectral satellite data (like Sentinel-2 or Landsat-8 data) with high revisiting frequency are suitable. Abdullah et al. (2019) evaluated Sentinel-2 and Landsat-8 for mapping green-attacked Norway spruce, with Sentinel-2 data giving promising results. However, due to deca-metric spatial resolution of the mentioned scanners (10–30 m), it is not possible to analyze individual trees. Such deca-metric data is hence only applicable when several adjacent trees are affected or when single trees are so strongly affected that they have a measurable impact on the entire pixel (Immitzer et al., 2016). Despite these difficulties, establishing a permanent monitoring system for detecting vitality changes in forests should be further pursued, including the analysis of the future spaceborne image spectrometer missions such as EnMAP (Guanter et al., 2015; Hill et al., 2019). Further, the new fleet of commercial satellites (e.g. 2nd generation Doves from Planet) should be examined as they offer daily acquisitions at metric spatial resolution – with however radiometric and spectral deteriorations.

The detected changes can help to identify hotspots which thereafter can be closer observed with data of even higher spatial resolution. Here, multispectral cameras mounted on unmanned aerial vehicles can be a valuable source, being applied in several forest related studies during the last years (Lehmann et al., 2015; Näsi et al., 2018; Nevalainen et al., 2017). UAV's main advantage is the extremely flexible operation – while costs are prohibitively high if used to monitor areas larger than a few hectares (Torresan et al., 2016). The use of UAV data is therefore only applicable for very small areas (<0.1–1 km^2). Probably, a synergetic use of freely available satellite data (for detecting hotspots within large areas) and low cost UAV (for confirmation and fine scale verification) is a promising approach. A combined use of free satellite data for "hot spot vitality change detection" together with UAVs for "verification" should be investigated as a future approach to detect and monitor tree vitality.

5. Conclusion

The hyperspectral data used in this study have a high potential for the detection of subtle changes in the reflection behavior of stressed trees. We monitored two forest stands over two vegetation periods, following a ring-barking. In the first vegetation period, the artificially stressed trees did not show any change. In the second year, the stress was detectable in the hyperspectral data, well before the changes were recognized during the field assessments.

It must be taken in consideration that the ground-based crown condition assessment has certain limitation (due to shadows, viewing angle etc.). If changes are not visible form the ground the tree can still be infested at that time. The spectral response of stressed trees was evident in both, needle and tree crown spectra.

The younger, more vital forest stand was more resistant to ring-barking than the older forest stand. In the latter, vitality changes were clearly visible in the hyperspectral data. In the second vegetation period some trees, mainly ring-barked trees, were infested by bark beetles, which led to the end of experiment. Those infested trees were spectrally different from the control trees. Primary trees with bark beetle infestation showed changes in the spectral behavior. It is not clear whether the reaction to the infestation or the predisposition is seen in the hyperspectral data. In any case the vitality change is visible well earlier in the spectral domain than in the field. Further research is needed to establish a better link between stress (predisposition) and bark beetle infestation.

Several optical features (spectra, derivatives, classical vegetation indices (VIs), angle indices and red edge parameters) were tested to detect changes of the reflection behavior of the stressed trees compared to the control trees. The spectra of the ring-barked trees changed in the visible, red-edge and SWIR range. For both needle and tree crown data, the derivatives, Red Edge Inflection parameter, as well as some VIs (especially PRI and MSRI) were reliable features to separate the two test groups.

The Random Forest (RF) models further confirmed the difference between the two groups as in the beginning of the second vegetation period the tree crown spectra of the two groups were already separated with 80% accuracy. Thereafter, the separability was even better and reached values >90%.

Remote sensing can help to detect changes from above earlier than from field. Which might be especially the case for six toothed bark beetles (*Pityogenes chalcographus*), which primary attacks the tree top of spruce forests.

Due to the high costs, airborne hyperspectral data acquisitions are only partially practicable. Also, the optimal timing of the flight is very difficult to coordinate. For this reason, satellites with high revisit frequency (like Sentinel-2 or Doves from Planet) are probably better suited for detecting hotspots within large areas. A synergetic use of this data with flexible and low cost UAV systems for confirmation and fine scale verification of the hot spots is a promising approach.

Declaration of Competing Interest

The authors declare that they have no known competing financial interests or personal relationships that could have appeared to influence the work reported in this paper.

Acknowledgements

The work has been partly supported by grants provided within the research project »VitTree: Automated assessment of forest tree vitality using up-to-date optical satellite data with enhanced spectral and spatial resolution« (E 54) funded by the Bavarian State Ministry of Food, Agriculture and Forestry. This support is greatly appreciated.

The authors thank the tree-climbing team, Alfred Wörle and his colleagues from LWF, as well as Wai-Tim Ng (BOKU) and Lea Henning (DLR) for the assistance in the field and in the spectral laboratory. We also thank Adelheid Wallner (LWF) for the organization of the needle sampling campaigns and Stephan Raspe (LWF) for the meteorological data. We thank Klaus Berneis (Bavarian State Forest enterprise) for the crown condition assessment. Further we thank DLR for funding and performing the flight campaign, for providing their spectral laboratory facilities in 2013 and for preprocessing the HySpex data (Martin Bachmann, Stefanie Holzwarth, Anne Reichmuth and Andreas Müller). The authors also thank the Bavarian State Forest enterprise for providing the test sites (Heinz Utschig, Matthias Frost, Bernhard Müller).

Open access funding provided by University of Natural Resources and Life Sciences Vienna (BOKU).

References

Abdullah, H., Darvishzadeh, R., Skidmore, A.K., Groen, T.A., Heurich, M., 2018. European spruce bark beetle (Ips typographus, L.) green attack affects foliar reflectance and biochemical properties. Int. J. Appl. Earth Obs. Geoinf. 64, 199–209. https://doi.org/10.1016/j.jag.2017.09.009.

Abdullah, H., Skidmore, A.K., Darvishzadeh, R., Heurich, M., 2019. Sentinel-2 accurately maps green-attack stage of European spruce bark beetle (Ips typographus, L.) compared with Landsat-8. Remote Sens. Ecol. Conserv. 5, 87–106. https://doi.org/10.1002/rse2.93.

Andreu, L., Gutierrez, E., Macias, M., Montse, R., Bosch, O., Camarero, J.J., 2007. Climate increases regional tree-growth variability in Iberian pine forests. Glob. Chang. Biol. 13, 804–815. https://doi.org/10.1111/j.1365-2486.2007.01322.x.

Atzberger, C., Eilers, P.H.C., 2011. Evaluating the effectiveness of smoothing algorithms in the absence of ground reference measurements. Int. J. Remote Sens. 32, 3689–3709. https://doi.org/10.1080/01431161003762405.

Atzberger, C., Zeug, G., Defourny, P., Aragão, L.E.O.C., Hammarström, L., Immitzer, M., 2020. Monitoring of Forests through Remote Sensing: Final Report. Europen Commision, Luxembourg. https://data.europa.eu/doi/10.2779/175242.

Bachmann, M., Habermeyer, M., Holzwarth, S., Richter, R., Müller, A., 2007. Including quality measures in an automated processing chain for airborne hyperspectral data. In: 5th EARSeL Workshop on Imaging Spectroscopy, Bruges, Belgium.

Barbosa, P.M., Grégoire, J.-M., Pereira, J.M.C., 1999. An algorithm for extracting burned areas from time series of AVHRR GAC data applied at a continental scale. Remote Sens. Environ. 69, 253–263. https://doi.org/10.1016/S0034-4257(99)00026-7.

Breiman, L., 2001. Random forests. Mach. Learn. 45, 5–32. https://doi.org/10.1023/A:1010933404324.

Brovkina, O., Cienciala, E., Zemek, F., Lukeš, P., Fabianek, T., Russ, R., 2017. Composite indicator for monitoring of Norway spruce stand decline. Eur. J. Remote Sens. https://doi.org/10.1080/22797254.2017.1372697.

Carter, G.A., 1994. Ratios of leaf reflectances in narrow wavebands as indicators of plant stress. Int. J. Remote Sens. https://doi.org/10.1080/01431169408954109.

Carter, G.A., Knapp, A.K., 2001. Leaf optical properties in higher plants: linking spectral characteristics to stress and chlorophyll concentration. Am. J. Bot. 88, 677–684. https://doi.org/10.2307/2657068.

Champagne, C., Pattey, E., Bannari, A., Stratchan, I.B., 2001. Mapping crop water status: issues of scale in the detection of crop water stress using hyperspectral indices. In: Proceedings of the 8th International Symposium on Physical Measurements and Signatures in Remote Sensing. https://www.academia.edu/18041715/Mapping_crop_water_stress_Issues_of_scale_in_the_detection_of_plant_water_status_using_hyperspectral_indices.

Chehata, N., Orny, C., Boukir, S., Guyon, D., Wigneron, J.P., 2014. Object-based change detection in wind storm-damaged forest using high-resolution multispectral images. Int. J. Remote Sens. 35, 4758–4777. https://doi.org/10.1080/01431161.2014.930199.

Cheng, T., Rivard, B., Sánchez-Azofeifa, G.A., Feng, J., Calvo-Polanco, M., 2010. Continuous wavelet analysis for the detection of green attack damage due to mountain pine beetle infestation. Remote Sens. Environ. 114, 899–910. https://doi.org/10.1016/j.rse.2009.12.005.

Coggins, S.B., Coops, N.C., Wulder, M.A., 2011. Estimates of bark beetle infestation expansion factors with adaptive cluster sampling. Int. J. Pest Manage 57, 11–21. https://doi.org/10.1080/09670874.2010.505667.

Datt, B., 1999. A new reflectance index for remote sensing of chlorophyll content in higher plants: tests using Eucalyptus leaves. J. Plant Physiol. 154, 30–36. https://doi.org/10.1016/S0176-1617(99)80314-9.

Daughtry, C.S.T., Walthall, C.L., Kim, M.S., De Colstoun, E.B., McMurtrey, J.E., 2000. Estimating corn leaf chlorophyll concentration from leaf and canopy reflectance. Remote Sens. Environ. https://doi.org/10.1016/S0034-4257(00)00113-9.

Dawson, T.P., Curran, P.J., 1998. A new technique for interpolating the reflectance red edge position. Int. J. Remote Sens. 19, 2133–2139. https://doi.org/10.1080/014311698214910.

Einzmann, K., Ng, W.-T., Immitzer, M., Pinnel, N., Atzberger, C., 2014. Method analysis for collecting and processing in-situ hyperspectral needle reflectance data for monitoring Norway spruce [Methodenanalyse zur Erfassung und Prozessierung hyperspektraler in-situ Nadelreflexionsdaten zum monitoring von Fichten]. Photogramm. Fernerkun 5, 423–434. https://doi.org/10.1127/1432-8364/2014/0234.

Einzmann, K., Immitzer, M., Böck, S., Bauer, O., Schmitt, A., Atzberger, C., 2017. Windthrow detection in European forests with very high-resolution optical data. Forests 8, 21. https://doi.org/10.3390/f8010021.

Elatawneh, A., Wallner, A., Manakos, I., Schneider, T., Knoke, T., 2014. Forest cover database updates using multi-seasonal RapidEye data—storm event assessment in the Bavarian Forest National Park. Forests 5, 1284–1303. https://doi.org/10.3390/f5061284.

Entcheva Campbell, P.K., Rock, B.N., Martin, M.E., Neefus, C.D., Irons, J.R., Middleton, E.M., Albrechtova, J., 2004. Detection of initial damage in Norway spruce canopies using hyperspectral airborne data. Int. J. Remote Sens. 25, 5557–5583. https://doi.org/10.1080/01431160410001726058.

Fajstavr, M., Giagli, K., Vavrčík, H., Gryc, V., Urban, J., 2017. The effect of stem girdling on xylem and phloem formation in Scots pine. Silva Fennica 51. https://doi.org/10.14214/sf.1760.

Fassnacht, F.E., Latifi, H., Koch, B., 2012. An angular vegetation index for imaging spectroscopy data—preliminary results on forest damage detection in the Bavarian National Park, Germany. Int. J. Appl. Earth Obs. Geoinf. 19, 308–321. https://doi.org/10.1016/j.jag.2012.05.018.

Fassnacht, F.E., Latifi, H., Ghosh, A., Joshi, P.K., Koch, B., 2014. Assessing the potential of hyperspectral imagery to map bark beetle-induced tree mortality. Remote Sens. Environ. 140, 533–548. https://doi.org/10.1016/j.rse.2013.09.014.

Fernandez-Carrillo, A., Patočka, Z., Dobrovolný, L., Franco-Nieto, A., Revilla-Romero, B., 2020. Monitoring bark beetle forest damage in Central Europe. A remote sensing approach validated with field data. Remote Sens. 12, 3634. https://doi.org/10.3390/rs12213634.

Foster, A.C., Walter, J.A., Shugart, H.H., Sibold, J., Negron, J., 2017. Spectral evidence of early-stage spruce beetle infestation in Engelmann spruce. For. Ecol. Manag. 384, 347–357. https://doi.org/10.1016/j.foreco.2016.11.004.

Fourty, T., Baret, F., Jacquemoud, S., Schmuck, G., Verdebout, J., 1996. Leaf optical properties with explicit description of its biochemical composition: direct and inverse problems. Remote Sens. Environ. https://doi.org/10.1016/0034-4257(95)00234-0.

Franklin, S.E., Wulder, M.A., Skakun, R.S., Carroll, A.L., 2003. Mountain pine beetle red-attack forest damage classification using stratified landsat TM data in British Columbia, Canada. Photogramm. Eng. Rem. Sen. 69, 283–288. https://doi.org/10.14358/PERS.69.3.283.

Gamon, J.A., Peñuelas, J., Field, C.B., 1992. A narrow-waveband spectral index that tracks diurnal changes in photosynthetic efficiency. Remote Sens. Environ. 41, 35–44. https://doi.org/10.1016/0034-4257(92)90059-S.

Gamon, J.A., Serrano, L., Surfus, J.S., 1997. The photochemical reflectance index: an optical indicator of photosynthetic radiation use efficiency across species, functional types, and nutrient levels. Oecologia 112, 492–501. https://doi.org/10.1007/s004420050337.

Gao, B., 1996. NDWI—A normalized difference water index for remote sensing of vegetation liquid water from space. Remote Sens. Environ. 58, 257–266. https://doi.org/10.1016/S0034-4257(96)00067-3.

Giglio, L., Loboda, T., Roy, D.P., Quayle, B., Justice, C.O., 2009. An active-fire based burned area mapping algorithm for the MODIS sensor. Remote Sens. Environ. 113, 408–420. https://doi.org/10.1016/j.rse.2008.10.006.

Gitas, I.Z., Polychronaki, A., Katagis, T., Mallinis, G., 2008. Contribution of remote sensing to disaster management activities: a case study of the large fires in the Peloponnese, Greece. Int. J. Remote Sens. 29, 1847–1853. https://doi.org/10.1080/01431160701874553.

Gitelson, A., Merzlyak, M.N., 1994. Spectral reflectance changes associated with autumn senescence of *Aesculus hippocastanum* L. and *Acer platanoides* L. leaves. Spectral features and relation to chlorophyll estimation. J. Plant Physiol. 143, 286–292. https://doi.org/10.1016/S0176-1617(11)81633-0.

Grabska, E., Socha, J., 2021. Evaluating the effect of stand properties and site conditions on the forest reflectance from Sentinel-2 time series. PLoS One 16, e0248459. https://doi.org/10.1371/journal.pone.0248459.

Guanter, L., Kaufmann, H., Segl, K., Foerster, S., Rogass, C., Chabrillat, S., Kuester, T., Hollstein, A., Rossner, G., Chlebek, C., Straif, C., Fischer, S., Schrader, S., Storch, T., Heiden, U., Mueller, A., Bachmann, M., Mühle, H., Müller, R., Habermeyer, M., Ohndorf, A., Hill, J., Buddenbaum, H., Hostert, P., Van der Linden, S., Leitão, P.J., Rabe, A., Doerffer, R., Krasemann, H., Xi, H., Mauser, W., Hank, T., Locherer, M., Rast, M., Staenz, K., Sang, B., 2015. The EnMAP spaceborne imaging spectroscopy mission for earth observation. Remote Sens. 7, 8830–8857. https://doi.org/10.3390/rs70708830.

Guyot, G., Baret, F., Major, D.J., 1988. High spectral resolution: determination of spectral shifts between the red and infrared. Int. Arch. Photogramm. Remote Sen. https://doi.org/10.1093/mind/VII.25.101.

Habermeyer, M., Müller, A., Holzwarth, S., Richter, R., Müller, R., Bachmann, M., Seitz, K.H., Seifert, P., Strobl, P., 2005. Implementation of the automatic processing chain for ARES. In: 4th EARSeL Workshop Imaging Spectroscopy, pp. 67–75. https://citeseerx.ist.psu.edu/viewdoc/download?doi=10.1.1.381.6950&rep=rep1&type=pdf.

Hardisky, M.A., Klemas, V., Smart, R.M., 1983. The influence of soil salinity, growth form, and leaf moisture on the spectral radiance of Spartina alterniflora canopies. Photogramm. Eng. Remote Sens. 49 (1), 77–83.

Havašová, M., Bucha, T., Ferenčík, J., Jakuš, R., 2015. Applicability of a vegetation indices-based method to map bark beetle outbreaks in the High Tatra Mountains. Ann. For. Res. 58, 295–310. https://doi.org/10.15287/afr.2015.388.

Hill, J., Buddenbaum, H., Townsend, P.A., 2019. Imaging spectroscopy of forest ecosystems: perspectives for the use of space-borne hyperspectral earth observation systems. Surv. Geophys. 40, 553–588. https://doi.org/10.1007/s10712-019-09514-2.

Holzwarth, S., Bachmann, M., Freer, M., Hofmann, M., 2011. Standards for airborne hyperspectral image data. In: 7th EARSeL Workshop Imaging Spectroscopy, pp. 1–7. Edinburgh, UK. https://elib.dlr.de/81790/1/S7_5_Holzwarth_paper.pdf.

Immitzer, M., Atzberger, C., 2014. Early detection of bark beetle infestation in Norway spruce (*Picea abies*, L.) using WorldView-2 data. Photogramm. Fernerkun 351–367. https://doi.org/10.1127/1432-8364/2014/0229.

Immitzer, M., Vuolo, F., Atzberger, C., 2016. First experience with sentinel-2 data for crop and tree species classifications in Central Europe. Remote Sens. 8, 1–27. https://doi.org/10.3390/rs8030166.

Immitzer, M., Lederbauer, S., Einzmann, K., Atzberger, C., 2017. Erkennung von Borkenkäferbefall mittels Unmanned Aerial Vehicle (UAV). Endbericht von StartClim2016.E, StartClim2016: Weitere Beiträge zur Umsetzung der österreichischen Anpassungsstrategie. BMLFUW, BMWF, ÖBf, Land Oberösterreich, Wien. https://docplayer.org/158770651-Startclim2016-e-erkennung-von-borkenkaeferbefall-mittels-unmanned-aerial-vehicle-uav-institut-fuer-vermessung-fernerkundung-und-landinformation.html.

Immitzer, M., Böck, S., Einzmann, K., Vuolo, F., Pinnel, N., Wallner, A., Atzberger, C., 2018. Fractional cover mapping of spruce and pine at 1ha resolution combining very

high and medium spatial resolution satellite imagery. Remote Sens. Environ. 204, 690–703. https://doi.org/10.1016/j.rse.2017.09.031.
Immitzer, M., Neuwirth, M., Böck, S., Brenner, H., Vuolo, F., Atzberger, C., 2019. Optimal input features for tree species classification in Central Europe based on multi-temporal sentinel-2 data. Remote Sens. 11, 2599. https://doi.org/10.3390/rs11222599.
Khanna, S., Palacios-Orueta, A., Whiting, M.L., Ustin, S.L., Riaño, D., Litago, J., 2007. Development of angle indexes for soil moisture estimation, dry matter detection and land-cover discrimination. Remote Sens. Environ. 109, 154–165. https://doi.org/10.1016/j.rse.2006.12.018.
Klouček, T., Komárek, J., Surový, P., Hrach, K., Janata, P., Vašíček, B., 2019. The use of UAV mounted sensors for precise detection of bark beetle infestation. Remote Sens. 11, 1561. https://doi.org/10.3390/rs11131561.
Köhler, C.H., 2016. Airborne imaging spectrometer HySpex. J. Large-Scale Res. Facil. 2, 1–6. https://doi.org/10.17815/jlsrf-2-151.
Krauß, T., d'Angelo, P., Schneider, M., Gstaiger, V., 2013. The Fully Automatic Optical Processing System CATENA at DLR. ISPRS - International Archives of the Photogrammetry. Remote Sensing and Spatial Information Sciences XL-1 (W1), 177–183. https://doi.org/10.5194/isprsarchives-XL-1-W1-177-2013.
Lausch, A., Heurich, M., Gordalla, D., Dobner, H.-J., Gwillym-Margianto, S., Salbach, C., 2013. Forecasting potential bark beetle outbreaks based on spruce forest vitality using hyperspectral remote-sensing techniques at different scales. For. Ecol. Manag. 308, 76–89. https://doi.org/10.1016/j.foreco.2013.07.043.
Lausch, A., Erasmi, S., King, D.J., Magdon, P., Heurich, M., 2016. Understanding forest health with remote sensing -part I—a review of spectral traits, processes and remote-sensing characteristics. Remote Sens. 8, 1029. https://doi.org/10.3390/rs8121029.
Lausch, A., Erasmi, S., King, D.J., Magdon, P., Heurich, M., 2017. Understanding forest health with remote sensing-part II—a review of approaches and data models. Remote Sens. 9, 129. https://doi.org/10.3390/rs9020129.
Lehmann, J.R.K., Nieberding, F., Prinz, T., Knoth, C., 2015. Analysis of unmanned aerial system-based CIR images in forestry—a new perspective to monitor Pest infestation levels. Forests 6, 594–612. https://doi.org/10.3390/f6030594.
Liaw, A., Wiener, M., 2002. Classification and regression by randomForest. R News 2, 18–22. https://cran.r-project.org/doc/Rnews/Rnews_2002-3.pdf.
LWF, 2012. Waldzustandserhebung in Bayern – Terrestrische Kronenzustandserhebung 2012. Freising.
LWF, 2014. Bayerische Waldklimastation Altötting. Bayerische Landesanstalt für Wald und Forstwirtschaft, Freising, Germany. https://www.lwf.bayern.de/mam/cms04/boden-klima/dateien/wks-altoetting_nbf.pdf.
McElhinny, C., Gibbons, P., Brack, C., Bauhus, J., 2005. Forest and woodland stand structural complexity: its definition and measurement. For. Ecol. Manag. 218, 1–24. https://doi.org/10.1016/j.foreco.2005.08.034.
Meddens, A.J.H., Hicke, J.A., Vierling, L.A., 2011. Evaluating the potential of multispectral imagery to map multiple stages of tree mortality. Remote Sens. Environ. 115, 1632–1642. https://doi.org/10.1016/j.rse.2011.02.018.
Meddens, A.J.H., Hicke, J.A., Vierling, L.A., Hudak, A.T., 2013. Evaluating methods to detect bark beetle-caused tree mortality using single-date and multi-date Landsat imagery. Remote Sens. Environ. 132, 49–58. https://doi.org/10.1016/j.rse.2013.01.002.
Meiforth, J.J., Buddenbaum, H., Hill, J., Shepherd, J., 2020. Monitoring of canopy stress symptoms in New Zealand kauri trees analysed with AISA hyperspectral data. Remote Sens. 12, 926. https://doi.org/10.3390/rs12060926.
Melillo, J.M., Aber, J.D., Muratore, J.F., 1982. Nitrogen and lignin control of hardwood leaf litter decomposition dynamics. Ecology. https://doi.org/10.2307/1936780.
Merzlyak, M.N., Gitelson, A.A., Chivkunova, O.B., Rakitin, V., 1999. Non-destructive optical detection of pigment changes during leaf senescence and fruit ripening. Physiol. Plant. 106, 135–141. https://doi.org/10.1034/j.1399-3054.1999.106119.x.
Moore, G.M., 2013. ing-barking and girdling: how much vascular connection do you need between roots and crown? Burnley College, University of Melbourne, Richmond. 3121 p.
Müller, R., Holzwarth, S., Habermeyer, M., Müller, A., 2005. Ortho image production within an automatic processing chain for hyperspectral airborne scanner ARES. In: Proceedings of the EARSeL Workshop 3D-Remote Sensing. Presented at the EARSeL Workshop 3D-Remote Sensing, Porto, Portugal. https://www.researchgate.net/profile/Rupert-Mueller/publication/224778397_Ortho_Image_Production_within_an_Automatic_Processing_Chain_for_hyperspectral_Airborne_Scanner_ARES/links/54986a6b0cf2c5a7e342bf44/Ortho-Image-Production-within-an-Automatic-Processing-Chain-for-hyperspectral-Airborne-Scanner-ARES.pdf.
Mutanga, O., Skidmore, A.K., 2007. Red edge shift and biochemical content in grass canopies. ISPRS J. Photogramm. Remote Sens. 62, 34–42. https://doi.org/10.1016/j.isprsjprs.2007.02.001.
Näsi, R., Honkavaara, E., Lyytikäinen-Saarenmaa, P., Blomqvist, M., Litkey, P., Hakala, T., Viljanen, N., Kantola, T., Tanhuanpää, T., Holopainen, M., 2015. Using UAV-based photogrammetry and hyperspectral imaging for mapping bark beetle damage at tree-level. Remote Sens. 7, 15467–15493. https://doi.org/10.3390/rs71115467.
Näsi, R., Honkavaara, E., Blomqvist, M., Lyytikäinen-Saarenmaa, P., Hakala, T., Viljanen, N., Kantola, T., Holopainen, M., 2018. Remote sensing of bark beetle damage in urban forests at individual tree level using a novel hyperspectral camera from UAV and aircraft. Urban For. Urban Green. 30, 72–83. https://doi.org/10.1016/j.ufug.2018.01.010.
Nevalainen, O., Honkavaara, E., Tuominen, S., Viljanen, N., Hakala, T., Yu, X., Hyyppä, J., Saari, H., Pölönen, I., Imai, N.N., Tommaselli, A.M.G., 2017. Individual tree detection and classification with UAV-based photogrammetric point clouds and hyperspectral imaging. Remote Sens. 9, 185. https://doi.org/10.3390/rs9030185.
Niemann, K.O., Quinn, G., Stephen, R., Visintini, F., Parton, D., 2015. Hyperspectral remote sensing of mountain pine beetle with an emphasis on previsual assessment. Can. J. Remote. Sens. 41, 191–202. https://doi.org/10.1080/07038992.2015.1065707.
Noel, A.R.A., 1970. The girdled tree. Bot. Rev. https://doi.org/10.1007/BF02858959.
Palacios-Orueta, A., Khanna, S., Litago, J., Whiting, M.L., Ustin, S.L., 2006. Assessment of NDVI and NDWI spectral indices using MODIS time series analysis and development of a new spectral index based on MODIS shortwave infrared bands. In: Proceedings of the 1st International Conference of Remote Sensing and Geoinformation Processing, pp. 207–209. https://blogs.upm.es/dynamicland/wp-content/uploads/sites/294/2019/06/Palacios_etal_2006.pdf.
Penuelas, J., Filella, I., Biel, C., Serrano, L., Save, R., 1993. The reflectance at the 950-970 nm region as an indicator of plant water status. Int. J. Remote Sens. https://doi.org/10.1080/01431169308954010.
Pereira, J.M.C., 2003. Remote sensing of burned areas in tropical savannas. Int. J. Wildland Fire 12, 259. https://doi.org/10.1071/WF03028.
R Core Team, 2017. R: a language and environment for statistical computing. R Foundation for Statistical Computing, Vienna, Austria.
Ratcliffe, S., Holzwarth, F., Nadrowski, K., Levick, S., Wirth, C., 2015. Tree neighbourhood matters – tree species composition drives diversity–productivity patterns in a near-natural beech forest. For. Ecol. Manag. 335, 225–234. https://doi.org/10.1016/j.foreco.2014.09.032.
Rautiainen, M., Stenberg, P., Nilson, T., Kuusk, A., 2004. The effect of crown shape on the reflectance of coniferous stands. Remote Sens. Environ. 89, 41–52. https://doi.org/10.1016/j.rse.2003.10.001.
Rautiainen, M., Lukeš, P., Homolová, L., Hovi, A., Pisek, J., Mõttus, M., 2018. Spectral properties of coniferous forests: a review of in situ and laboratory measurements. Remote Sens. 10, 207. https://doi.org/10.3390/rs10020207.
Reichmuth, A., Henning, L., Pinnel, N., Bachmann, M., Rogge, D., 2018. Early detection of vitality changes of multi-temporal Norway spruce laboratory needle measurements—the ring-barking experiment. Remote Sens. 10, 57. https://doi.org/10.3390/rs10010057.
Richter, R., Schläpfer, D., Müller, A., 2011. Operational atmospheric correction for imaging spectrometers accounting for the smile effect. IEEE T Geosci. Remote 49, 1772–1780. https://doi.org/10.1109/TGRS.2010.2089799.
Rock, B.N., Hoshizaki, T., Miller, J.R., 1988. Comparison of in situ and airborne spectral measurements of the blue shift associated with forest decline. Remote Sens. Environ. https://doi.org/10.1016/0034-4257(88)90008-9.
Roth, B., Bucher, H.-U., Schütz, J.-P., Ammann, P., 2001. Ringeln – Alte Methode neu angewendet. Wald und Holz 38–41. http://www.gebirgswald.ch/tl_files/gebirgswald/de/05_Wald_u_Holz/2001_04_Artikel_Wald_Holz_Ringeln.pdf.
Rouse, Rouse, Jr, J.W., Haas, R.H., Schell, J.A., Deering, D.W., 1974. Monitoring vegetation systems in the great plains with ERTS. In: Proceedings of the Third ERTS-1 Symposium; NASA SP-351. NASA, Washington, DC, USA, pp. 309–317. https://ntrs.nasa.gov/api/citations/19740022614/downloads/19740022614.pdf.
Roy, D.P., Jin, Y., Lewis, P.E., Justice, C.O., 2005. Prototyping a global algorithm for systematic fire-affected area mapping using MODIS time series data. Remote Sens. Environ. 97, 137–162. https://doi.org/10.1016/j.rse.2005.04.007.
Rullan-Silva, C.D., Olthoff, A.E., Delgado de la Mata, J.A., Pajares-Alonso, J.A., 2013. Remote monitoring of forest insect defoliation. A review. For. Syst. 22, 377–391. https://doi.org/10.5424/FS/2013223-04417.
Safonova, A., Tabik, S., Alcaraz-Segura, D., Rubtsov, A., Maglinets, Y., Herrera, F., 2019. Detection of fir trees (*Abies sibirica*) damaged by the bark beetle in unmanned aerial vehicle images with deep learning. Remote Sens. 11, 643. https://doi.org/10.3390/rs11060643.
Schlerf, M., Atzberger, C., 2006. Inversion of a forest reflectance model to estimate structural canopy variables from hyperspectral remote sensing data. Remote Sens. Environ. 100, 281–294. https://doi.org/10.1016/j.rse.2005.10.006.
Seidl, R., Thom, D., Kautz, M., Martin-Benito, D., Peltoniemi, M., Vacchiano, G., Wild, J., Ascoli, D., Petr, M., Honkaniemi, J., Lexer, M.J., Trotsiuk, V., Mairota, P., Svoboda, M., Fabrika, M., Nagel, T.A., Reyer, C.P.O., 2017. Forest disturbances under climate change. Nat. Clim. Chang. 7, 395–402. https://doi.org/10.1038/nclimate3303.
Seidl, R., Honkaniemi, J., Aakala, T., Aleinikov, A., Angelstam, P., Bouchard, M., Boulanger, Y., Burton, P.J., Grandpré, L.D., Gauthier, S., Hansen, W.D., Jepsen, J.U., Jögiste, K., Kneeshaw, D.D., Kuuluvainen, T., Lisitsyna, O., Makoto, K., Mori, A.S., Pureswaran, D.S., Shorohova, E., Shubnitsina, E., Taylor, A.R., Vladimirova, N., Vodde, F., Senf, C., 2020. Globally consistent climate sensitivity of natural disturbances across boreal and temperate forest ecosystems. Ecography 43, 967–978. https://doi.org/10.1111/ecog.04995.
Senf, C., Seidl, R., Hostert, P., 2017. Remote sensing of forest insect disturbances: current state and future directions. Int. J. Appl. Earth Obs. Geoinf. 60, 49–60. https://doi.org/10.1016/j.jag.2017.04.004.
Serrano, L., Peñuelas, J., Ustin, S.L., 2002. Remote sensing of nitrogen and lignin in Mediterranean vegetation from AVIRIS data: decomposing biochemical from structural signals. Remote Sens. Environ. https://doi.org/10.1016/S0034-4257(02)00011-1.
Seybold, S.J., Paine, T.D., Dreistadt, S.H., 2008. Bark beetles: integrated pest management for home gardeners and landscape professionals. Pest Notes Univ. Calif. Agric. Nat. Resour. 7421, 1–7. http://ipm.ucanr.edu/PDF/PESTNOTES/pnbarkbeetles.pdf.
Sims, D.A., Gamon, J.A., 2002. Relationships between leaf pigment content and spectral reflectance across a wide range of species, leaf structures and developmental stages. Remote Sens. Environ. 81, 337–354. https://doi.org/10.1016/S0034-4257(02)00010-X.

Slonecker, T., 2011. Analysis of the Effects of Heavy Metals on Vegetation Hyperspectral Reflectance Properties, pp. 561–578. https://doi.org/10.1201/b11222-33.

Smith, R.C.G., Adams, J., Stephens, D.J., Hick, P.T., 1995. Forecasting wheat yield in a Mediterranean-type environment from the NOAA satellite. Aust. J. Agric. Res. https://doi.org/10.1071/AR9950113.

Torresan, C., Berton, A., Carotenuto, F., Gennaro, S.F.D., Gioli, B., Matese, A., Miglietta, F., Vagnoli, C., Zaldei, A., Wallace, L., 2016. Forestry applications of UAVs in Europe: a review. Int. J. Remote Sens. 1–21. https://doi.org/10.1080/01431161.2016.1252477.

Tsai, F., Philpot, W., 1998. Derivative analysis of hyperspectral data. Remote Sens. Environ. https://doi.org/10.1016/S0034-4257(98)00032-7.

Weirather, M., Zeug, G., Schneider, T., 2018. Automated delineation of wildfire areas using sentinel-2 satellite imagery. Giforum 1, 251–262. https://doi.org/10.1553/giscience2018_01_s251.

Wermelinger, B., 2004. Ecology and management of the spruce bark beetle Ips typographus—a review of recent research. For. Ecol. Manag. 202, 67–82. https://doi.org/10.1016/j.foreco.2004.07.018.

Widlowski, J.-L., Mio, C., Disney, M., Adams, J., Andredakis, I., Atzberger, C., Brennan, J., Busetto, L., Chelle, M., Ceccherini, G., Colombo, R., Côté, J.-F., Eenmäe, A., Essery, R., Gastellu-Etchegorry, J.-P., Gobron, N., Grau, E., Haverd, V., Homolová, L., Huang, H., Hunt, L., Kobayashi, H., Koetz, B., Kuusk, A., Kuusk, J., Lang, M., Lewis, P.E., Lovell, J.L., Malenovský, Z., Meroni, M., Morsdorf, F., Mõttus, M., Ni-Meister, W., Pinty, B., Rautiainen, M., Schlerf, M., Somers, B., Stuckens, J., Verstraete, M.M., Yang, W., Zhao, F., Zenone, T., 2015. The fourth phase of the radiative transfer model intercomparison (RAMI) exercise: actual canopy scenarios and conformity testing. Remote Sens. Environ. 169, 418–437. https://doi.org/10.1016/j.rse.2015.08.016.

Wulder, M.A., White, J.C., Bentz, B., Alvarez, M.F., Coops, N.C., 2006. Estimating the probability of mountain pine beetle red-attack damage. Remote Sens. Environ. 101, 150–166. https://doi.org/10.1016/j.rse.2005.12.010.

Wulder, M.A., White, J.C., Carroll, A.L., Coops, N.C., 2009. Challenges for the operational detection of mountain pine beetle green attack with remote sensing. For. Chron. 85, 32–38. https://doi.org/10.5558/tfc85032-1.

Zimmermann, S., Hoffmann, K., 2020. Evaluating the capabilities of Sentinel-2 data for large-area detection of bark beetle infestation in the Central German Uplands. JARS 14, 024515. https://doi.org/10.1117/1.JRS.14.024515.